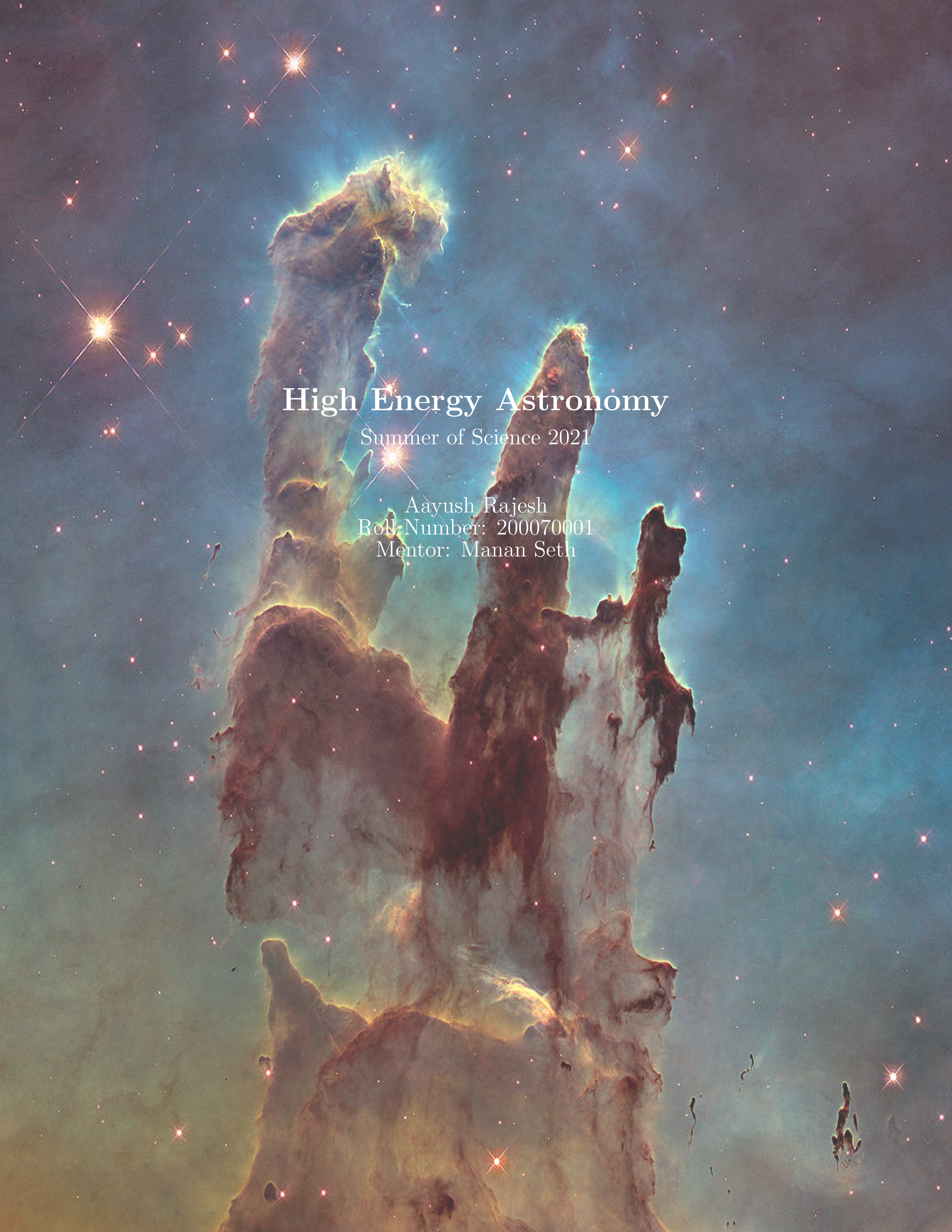

High Energy Astronomy

Summer of Science 2021

Aayush Rajesh
Roll Number: 200070001
Mentor: Manan Seth

Contents

Chapter 1

Introduction

The end of the Second World War was the dawn of a new age for astronomy and astrophysics. With the advent of new techniques and technologies, there have been dramatic advances in astronomy and the emergence of newer fields. One of the most important newer fields, was *high energy astrophysics*.

High energy astrophysics, as the name suggests, deals with the physics of high energy processes in astronomical environments. It exposes us to the tumultuous environments of stars, the extreme nature of black holes, the highly energetic magnetic fields of neutron stars, to name a few, with more mysteries yet to be understood.

1.1 History

The launch-pad for this field was the opening up of the entire electromagnetic spectrum for astronomical observations. Until the World War, astronomy was synonymous with optical astronomy, i.e. observations carried out with visible light. With advancements in technology, the other regions of the electromagnetic spectrum were unlocked for observation.

Infrared Waveband
Interstellar extinction is the absorption and scattering of radiation by dust and gas between the astronomical source and the observer. While the visible waveband is susceptible to extinction, the dust is transparent to the infrared waveband. Images of the sky in the near-infrared waveband have reduced extinction due to interstellar dust and have revealed the structure of our galaxy. Surveys conducted by 2MASS and COBE have revealed the central regions of our galaxy, the important star formation regions, which were enshrouded in dust. These observations provided convincing evidence for the presence of a supermassive black hole, called *Sagittarius A**, at the Galactic Core.

Radio Waveband
Radio emissions have been discovered from a wide range of different astronomical objects. The processes pertaining to these radio emissions were many, but the most common one was the synchroton radiation of ultra-relativistic electrons in magnetic fields. These radio observations have provided us information about the hottest plasmas in the universe. Observation of radio sources have led to the discovery of *quasars* (*quasi-stellar radio sources*) and a kind of neutron star known as *radio*

Figure 1.1: Galactic Core in infrared as observed by NASA's Spitzer Space Telescope.

pulsars, the first definitive proof of the existence of these stars.

X-Ray Waveband
With rockets lifting payload detectors above the atmosphere, X-Ray astronomy has uncovered a number of stellar X-ray sources, discovering pulsating sources associated with neutron stars, as well as X-ray emission due to accretion of matter by black holes in binary star systems. It has also led to the identification of clusters of galaxies, whose nuclei house intense, and often variable, X-ray sources.

γ-Ray Waveband
γ-Rays are highly energetic, with energies greater than 100keV. Very high energy γ-rays can initiate photon-electron electromagnetic cascades in the upper atmosphere, and the ultra-relativistic particles produced can generate Cherenkov radiation which can be observed from the ground level. Gamma ray bursts originating from violent events involving stellar-mass objects, and the subsequent afterglow observed in the rest of the electromagnetic spectrum, are of significant cosmological importance.

Cosmic Rays
The discovery of cosmic rays hinted at another facet to the Universe apart from just stars and interstellar gas. Cosmic radiation consisted of high energy particles of chemical composition similar to that of the sun, and the ionisation effect at the top of the atmosphere by very high energy cosmic rays, led to extensive air showers of products of this ionisation, thus providing a means of detection. Cosmic rays had profound implications to particle physics, as the detection of these air showers led to the discovery *muons, kaons* and *pions*, verifying Yukawa's theoretical predictions.

1.2 Non-Electromagnetic Astronomy

Neutrino Astrophysics

The discovery of *neutrinos* originating from the Sun as a part of the solar neutrino experiment matched predictions by one of the best solar models of the time. However, the detected neutrinos were only a fraction of what was predicted by the models, leading to what was termed as the *solar neutrino paradox*. This deficit was later accounted for by the discovery that neutrinos have finite rest masses. Neutrinos have also been detected from supernovae leading to the formation of neutron stars, thus providing insights into the physical processes involved.

Gravitational Waves

Gravitational waves are predicted to exist by Einstein's Theory of Relativity, however they are expected to be weak due to the weak nature of the gravitational force as compared to the other fundamental forces. The LIGO project (Laser Interferometer Gravitational Wave Observatory) has detected binary black hole mergers as well as neutron star mergers, in accordance with theory, and have provided information about the nature (mass, spin etc.) of the merging bodies involved.

Chapter 2

Stellar Astrophysics

Stars are the most widely recognized astronomical objects, with over a *100 billion* stars residing in our Milky Way alone, each having a variety of properties and behaviours. The study of stars is key to astronomy, for it helps us to uncover a wide range of physical processes key to their evolution.

2.1 Origin

When non-uniformity develops in massive interstellar gas clouds, gravitational instability leads to these "pockets" of higher densities accumulating more matter from the cloud. Large-scale gravitational instability developed in the central regions of this gas cloud can trigger gravitational collapse. The collapsing gas releases its gravitational potential energy as heat, which results in the formation of a superhot, rotating ball of gas known as a **protostar**. The protostar continues to accrete matter from the surrounding cloud, until core temperature is high enough to initiate nuclear fusion of hydrogen, at which point it is called a star. Often, star formation is widespread, in "stellar nurseries" - regions of massive molecular clouds.

Figure 2.1: Star formation in the stellar nursery NGC 346 observed by NASA's Hubble Telescope.

2.2 Hertzsprung-Russel Diagram

The Hertzsprung-Russel Diagram (HR Diagram), also known as the *color-magnitude diagram*, serves as an important tool to study stellar evolution. E. Hertzsprung and H.N. Russel independently noticed a correlation between the spectral type and intrinsic luminosities of stars in the scatter plot. By relating two of the fundamental physical parameters of stars, we can identify a star's evolutionary stage just from it's position on the diagram. From Figure 2.2, we can identify a few key patterns:

- A vast majority of the stars, including our Sun, lie along a diagonal, narrow and long band. This band of stars is known as the *Main sequence*.
- Lying above the main sequence are the *giants, bright giants* and *super giants*. These are stars that belong to the same spectral class but have higher luminosities and are hence, much bigger than main sequence stars.
- Lying below the main sequence, on the lower left, are the *white dwarfs*. These faint stars have high temperatures, implying that they are much smaller than main sequence stars.
- There also exists a region between the giant branch and the main sequence that is almost devoid of stars, known as the *Hertzsprung Gap*.

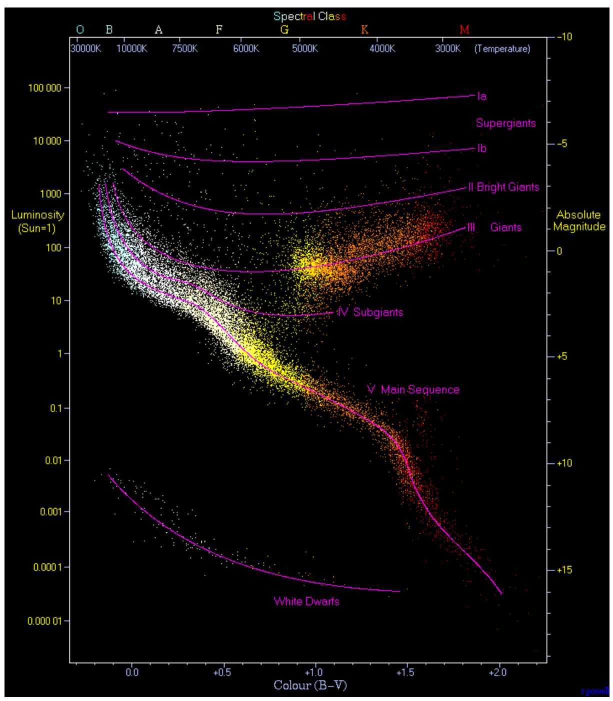

Figure 2.2: A HR Diagram of 22,000 stars plotted from the Hipparcos Catalogue.

2.3 Equations of Stellar Structure

We shall now try to describe the interior of a star. Under the assumption that the evolution of the star is slow, i.e. the star is *quasi-static*, and that the star is spherically symmetric and homogeneous, devoid of any rotation, we can come up with **four** differential equations of stellar structure, which, when put together with an *equation of state* for the of the material in the star, can provide a description of the nature of the star. The four equations are: (i) equation of hydrostatic support (2.3), (ii) law of conservation of mass (2.5), (iii) equation of energy generation (2.12), and (iv) equation of radiative transport (2.17).

2.3.1 Equation of Hydrostatic Support

Consider a star of mass M_T and radius R. Taking $M(r)$ to be the mass of the star contained within a radius r, and $\rho(r)$ to be the density of the material in the star, consider the forces on a cuboid at a radius r, of area dA and thickness dr

$$F_{gr} = \frac{GM(r)m}{r^2} = \frac{GM(r)\rho(r)\,dA\,dr}{r^2} \tag{2.1}$$

$$F_p = dA[p(r) - p(r+dr)] = -dA\,dr\,\frac{dp}{dr} \tag{2.2}$$

For the star to remain in equilibrium, we balance the two forces, and arrive at the *equation of hydrostatic support*:

$$\frac{dp}{dr} = -\frac{GM(r)\rho(r)}{r^2} \tag{2.3}$$

2.3.2 Equation of Mass Conservation

The mass contained in a spherical shell between the radii r and $r +$ dr is given by

$$M(r+dr) - M(r) = dM = 4\pi r^2 \rho(r)\,dr \tag{2.4}$$

Which, upon rearranging, gives us the *equation of mass conservation*

$$\frac{dM}{dr} = 4\pi r^2 \rho(r) \tag{2.5}$$

Using the two equations that we have derived, we can perform some interesting calculations. Dividing equations (2.3) and (2.5), we get

$$\frac{dp}{dM} = -\frac{GM}{4\pi r^4} \tag{2.6}$$

Now, integrating this from the centre to the surface of the star

$$-\int_0^{M_T} \frac{dp}{dM}\,dM = p_{centre} - p_{surface} = \int_0^{M_T} \frac{GM}{4\pi r^4}\,dM$$

Plugging in values for our Sun, taking $p_{surface} = 0$ and *underestimating* the integral by taking $r = R_\odot$, we get

$$p_{surface} > \frac{G{M_\odot}^2}{8\pi {R_\odot}^4} = 4.5 \times 10^8 \text{ atmospheres}$$

This rough calculation gives us the notion of how high the pressure at the centre of the Sun is.

2.3.3 The Virial Theorem: A Detour

From the two equations of stellar structure that we have derived so far, we can derive the *virial theorem for stars*, which is one of the most important equations for understanding the structure and evolution of a star.

Reorganizing equation (2.6),

$$4\pi r^3\, dp = 3V\, dp = -\frac{GM}{r}\, dM \tag{2.7}$$

where V denotes volume of the star. Integrating the expression from the centre to the surface of the star, and performing integration-by-parts,

$$3\int_{p_{centre}}^{p_{surface}} p\, dV + \Omega = 0$$

Here Ω represents the *gravitational potential energy* of the star, and is a negative quantity. Finally, using $dM = \rho\, dV$, we arrive at the *virial theorem*,

$$3\int_0^{M_T} \frac{p}{\rho}\, dM + \Omega = 0 \tag{2.8}$$

Using the relation between the internal energy per unit volume and pressure of an ideal gas of adiabatic exponent γ,

$$u = \frac{p}{\gamma - 1}$$

we can arrive at a more useful form of the virial theorem

$$3(\gamma - 1)U + \Omega = 0 \tag{2.9}$$

where U is the total internal energy of the star. For monoatomic gases (which are the primary components of a star), $\gamma = 5/3$, which gives us

$$2U + \Omega = 0 \tag{2.10}$$

Equation (2.10) proves to be a resolution to the *thermal paradox for stars*, which states that as stars radiate energy, they heat up. As stars lose energy, the total energy $E = U + \Omega = -U$ becomes more negative, and hence, the internal energy increases leading to a rise in temperature.

We can also estimate the *Kelvin-Helmholtz* or *thermal-time scale for stars*, which is the time it would take for a star to radiate away all it's internal thermal energy. For the Sun:

$$t_{KH} = \frac{U}{L_\odot} \approx \frac{G{M_\odot}^2}{2R_\odot L_\odot} = 1.5 \times 10^7 \text{ years}$$

where $L_\odot$ is the luminosity of the Sun. From the knowledge that the age of the Earth is 4.5 billion years, the estimate of 1.5 million years for the Sun's entire lifespan is off. This is because we have not considered the nuclear energy source in the Sun's core.

The virial theorem also ensures the stability of nuclear burning. If the equilibrium burning rate of nuclear fuel in the core of the star ϵ changes by an amount $\Delta\epsilon$, the increased production of energy causes the star to expand, making Ω less negative, causing U to decrease, thereby cooling the core. Since energy production is temperature dependent, this reduces the burning rate back to equilibrium. Thus, the virial theorem ensures a *strong negative feedback loop* in non-degenerate stars, making nuclear burning stable. Note that this is **not** the case when the matter in the star is degenerate, as pressure is now independent of temperature, and the star does not expand due to the perturbation. Therefore the temperature of the core further increases, causing a *positive feedback loop*, which can lead to thermonuclear runaway, something we shall touch upon while discussing mass loss in stars.

2.3.4 Equation of Energy Generation

The contribution to the total energy outflow from a star, by a spherical shell of radius r and thickness dr is

$$dL = 4\pi r^2 \rho\, \epsilon\, dr \tag{2.11}$$

where ϵ is the rate of energy generated by nuclear processes per unit mass of stellar matter, and is dependent on local temperature, density and chemical composition. Rearranging, we arrive at the *equation of energy generation*:

$$\frac{dL}{dr} = 4\pi r^2 \rho\, \epsilon \tag{2.12}$$

The derived form of the equation represents the convenient form of thermal equilibrium condition in stellar interior during the phases in which the star spends a sufficiently long time. There are critical phases of stellar life, however, when other sources of energy, like gravitational and thermal, play an important role in supplementing the role of nuclear energy. During these phases, the star adjusts its structure by expanding or contracting in order to achieve stability again. During such phases, the equation takes the form

$$\frac{dL}{dr} = 4\pi r^2 \rho \left(\epsilon - T\frac{dS}{dt} \right) \tag{2.13}$$

where S is the entropy of the star. Here, the latter term in the brackets represents the gravitational energy generation rate, which describes the energy change due to contraction or expansion of the star. During the non-critical (constant) phase of stellar life, the contribution from this term is negligible.

In main sequence stars, the main source of energy is the nuclear reaction converting hydrogen to helium. This conversion can take place through two processes:

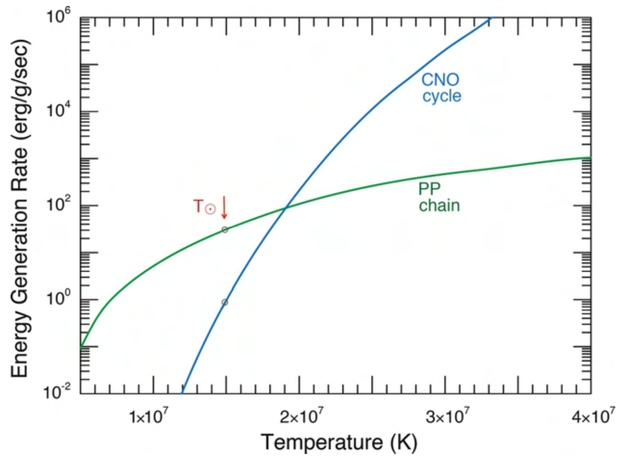

Figure 2.3: Temperature dependence of nuclear energy generation for P-P chain and CNO cycle.

- The *proton-proton (p-p) chain reaction* is the dominant form of energy generation for temperatures lower than 1.7×10^7 K. The energy generation rate can be described by $\epsilon \propto T^4$. Principal reactions involved are:

$$\mathrm{p} + \mathrm{p} \longrightarrow {}^2_1\mathrm{H} + \mathrm{e}^+ + \nu_e$$
$${}^2_1\mathrm{H} + \mathrm{p} \longrightarrow {}^3_2\mathrm{He} + \gamma$$
$${}^3_2\mathrm{He} + {}^3_2\mathrm{He} \longrightarrow {}^4_2\mathrm{He} + 2\,\mathrm{p}$$

  The detection of the electron neutrinos (ν_e) produced in the second reaction is a key test of this theory.

- The *CNO cycle* is the dominant energy generation pathway for temperatures greater than 1.7×10^7 K. It involves the successive addition of protons to nuclei and the use of Carbon as a catalyst. The energy generation rate can be described by $\epsilon \propto T^{17}$. Reactions involved are:

$${}^{12}_{6}\mathrm{C} + \mathrm{p} \longrightarrow {}^{13}_{7}\mathrm{N} + \gamma$$
$${}^{13}_{7}\mathrm{N} \longrightarrow {}^{13}_{6}\mathrm{C} + \mathrm{e}^+ + \nu_e$$
$${}^{13}_{6}\mathrm{C} + \mathrm{p} \longrightarrow {}^{14}_{7}\mathrm{N} + \gamma$$
$${}^{14}_{7}\mathrm{N} + \mathrm{p} \longrightarrow {}^{15}_{8}\mathrm{O} + \gamma$$
$${}^{15}_{8}\mathrm{O} \longrightarrow {}^{15}_{7}\mathrm{N} + \mathrm{e}^+ + \nu_e$$
$${}^{15}_{7}\mathrm{N} + \mathrm{p} \longrightarrow {}^{4}_{2}\mathrm{He} + {}^{12}_{6}\mathrm{C}$$

2.3.5 Equation of Radiative Transport

Energy transport through a star can occur through any of three ways: *conduction, convection and radiation*. Despite the fact that radiation undergoes heavy scattering in the interior of stars, it is still much more important than thermal conduction. This is because the mean free path of photons, although small, is much larger than that of particles like electrons. This results in photons, which undergo a *random walk process*, carrying most of the energy flux. This, however, is not the case in stars with degenerate matter, where conduction by electrons is very efficient. Convection, on the other hand, take over energy transport only when the temperature gradient exceeds the adiabatic gradient (a condition known as *super-adiabatic*).

We shall focus primarily on radiative transport in stars. The standard form of the heat diffusion equation is

$$F = -\lambda \frac{dT}{dr} \tag{2.14}$$

where F is the power per unit area parallel to temperature gradient. Therefore luminosity $L = 4\pi r^2 F$. Also, the change in radiation pressure

$$dp = -\frac{\kappa \rho F}{c}\, dr \tag{2.15}$$

where κ is the *opacity* of stellar material and represents the fraction of the flux absorbed or scattered per unit length per unit mass. We can also show, from Stefan-Boltzmann Law, that radiation pressure is given by $p = \frac{1}{3} a T^4$, where $a = \frac{4\sigma}{c}$. So,

$$\frac{dp}{dT} = \frac{dp}{dr}\frac{dr}{dT} = \frac{4}{3} a T^3$$

Substituting appropriate expressions for the derivatives, we get

$$F = -\frac{4}{3}\frac{acT^3}{\kappa\rho}\frac{dT}{dr} \tag{2.16}$$

which upon expressing in terms of luminosity gives us the *equation of radiative transport*:

$$\frac{dT}{dr} = \frac{3\kappa\rho}{16\pi a c r^2 T^3} L \tag{2.17}$$

The following table lists the physical processes behind opacity in different temperature ranges:

Temperature	Range	Physical Process
Low	$10^4 - 10^{4.5}$	Atomic and molecular absorption
Medium	$10^{4.5} - 10^7$	Bound-free and free-free absorption
High	$> 10^7$	Electron scattering

2.4 Stellar Structure

Models of quasi-static stars can be created by pairing the equations of stellar structure with the equation of state of the star. Some basic insights into the stellar interior can be drawn by adopting a *homologous stellar model*, under the assumptions that the composition of the star is homogeneous and the properties of energy transport and generation are universal within the star. Under these assumptions, the four equations, paired with the equation of state corresponding to an ideal gas, can be used to obtain power-law relations describing the dependence of the properties of stars. However, we must understand that more accurate models arise from taking into consideration non idealities of the stellar structure, such as: non-homogeneity, effects of convective regions in the star and the detailed physics of nuclear energy generation and radiation.

Schönberg and Chandrashekhar discovered in 1942 that stellar models with an inert core containing more than 10% to 15% of the mass of the star are unstable. In such cases, the hydrogen-burning shell surrounding the inert helium core experiences a very high pressure, causing the inner regions to collapse. The collapse continues until helium fusion begins in the core.

We can also arrive at a better estimate at the lifetime of a star. The fraction of rest mass converted to energy due to either the p-p chain or CNO cycle is 0.007. Also, stars move off the main-sequence of the HR diagram when the Schönberg-Chandrashekhar limit is reached (mass of core is 10% of mass of star). Hence, the main sequence lifetime of a star is given by:

$$T_{MS} = \frac{E}{L} = \frac{0.007(0.1 \times M)c^2}{L}$$

For the Sun, this comes out to be 10^{10} years. From the mass-luminosity relation $L \propto M^x$ where $x \sim 3.5$ for stars with $M \sim M_\odot$, the main-sequence lifetime for a star is:

$$T(M) = 10^{10} \left(\frac{M}{M_\odot}\right)^{1-x} \text{ years} \tag{2.18}$$

2.5 Stellar Evolution

2.5.1 Hayashi Track

When a protostar is forming by accumulation of matter from the surrounding enevelope of interstellar dust and gas, it is not yet on the main-sequence, and is known as a *pre-main-sequence star* (PMS). After accumulating most of its mass from the molecular cloud, it blows off the remaining envelope. At this point, fusion has not begun in the core, and hence, the main source of energy is gravitational contraction as opposed to hydrogen burning. At this point of contraction, the PMS is said to have "taken birth" on the HR diagram and proceeds along the *Hayashi Track*.

Hayashi showed that before the protostar can achieve hydrostatic equilibrium, the surface temperature must be sufficiently high. Also, the high opacity of the interior of the star prevents the smooth transfer of radiation, which results in large scale convection currents throughout the star carrying energy to the surface. The Hayashi track thus describes a fully convective star, or rather, a super-adiabatic one. The mathematical condition for this state is given by:

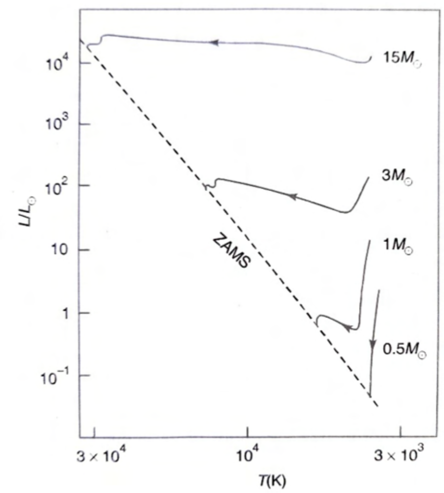

Figure 2.4: Evolution of PMS stars of different masses on HR diagram.

$$\frac{\mathrm{d}\ \ln T}{\mathrm{d}\ \ln P} \geq \frac{\gamma - 1}{\gamma} \tag{2.19}$$

It has also been shown by Hayashi that during this stage of convective equilibrium, the contraction of the star continues keeping the surface temperature almost constant. Thus, the luminosity of the star decreases, and the star descends vertically down the HR diagram. As the star contracts, the radiative region grows until the convective region is confined to the envelope (in low mass stars) or is entirely pushed out (in high mass stars).

The contraction of the star continues until nuclear energy generation is sufficient to balance stellar radiation, and at this point the star settles on the main sequence. As seen from Figure 2.4, high mass stars achieve radiative equilibrium quickly, and hence have a smaller vertical descent, at which point they follow the *Henyey Track*: a period of rapidly rising temperature at nearly constant luminosity. The region to the right of the Hayashi track is known as the **Forbidden Zone**, a region where no star can exist in stable hydrostatic equilibrium. This region is unstable as stars belonging here have:

$$\frac{\mathrm{d}\ \ln T}{\mathrm{d}\ \ln P} > 0.4$$

where 0.4 is the threshold for super-adiabatic nature as obtained by putting $\gamma = 5/3$ for monoatomic gas in equation (2.19).

2.5.2 Low Mass Stars

After reaching the main sequence, low mass stars continue burning the hydrogen in the core. After depleting all the hydrogen in the core (a process which takes a very long time), hydrogen burning continues in a shell surrounding the helium core. The shell starts thinning, but the star becomes brighter and grows in size, while seeing a reduction in surface temperature. Thus, the star ascends the red-giant branch, moving towards the top-right of the HR diagram. Even along the red-giant branch, these stars see a significant mass loss, as the outer, weakly held, layers of the star are blown off by strong radiation forces.

As the star ascends the branch, the core becomes hotter, denser and increasingly degenerate. In such conditions, conduction of heat by electrons is far more efficient than convection or radiation. Once the temperature of the core is hot enough to initiate helium burning, a very brief runaway thermonuclear reaction is achieved, and the core burns up almost all of its helium, at an exponentially increasing fusion rate comparable to that of the entire Milky Way. This is known as the **helium flash**, and most of the energy alleviates the core of degeneracy and drives off some of the outer layers. In very low mass stars (less than $0.5M_{\odot}$) core temperatures are not high enough, and the degenerate helium core continues contracting, to form a *helium white dwarf*.

Following the helium flash, normal helium burning continues in the core at a gradual pace. On the HR Diagram, the star is now a part of the *red clump*. Once helium in the core is exhausted, hydrogen and helium burning continues in shells surrounding the inert carbon-oxygen (CO) core. At this point, the star ascends the *asymptotic giant branch*. The burning in the two shells do not occur simultaneously, but alternate with each other, causing **thermal pulses**. The thermal pulses drive off significant amounts of stellar mass. What remains is the exposed core, which cools, becomes degenerate, and turns into a *white dwarf*, and the ejected envelope surrounding the core, which is ionised by the white dwarf and is called a *planetary nebula*.

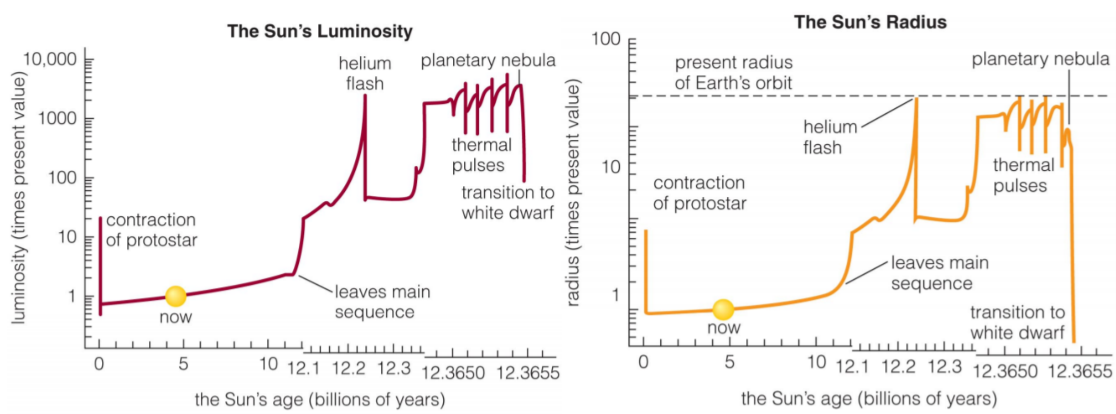

Figure 2.5: Evolution in size and luminosity of a Sun-like star.

2.5.3 High Mass Stars

Massive stars burn hydrogen in their cores via the CNO cycle, and the steep temperature gradient makes the core convective instead of radiative. Hence, depletion of nuclear fuel is much faster in

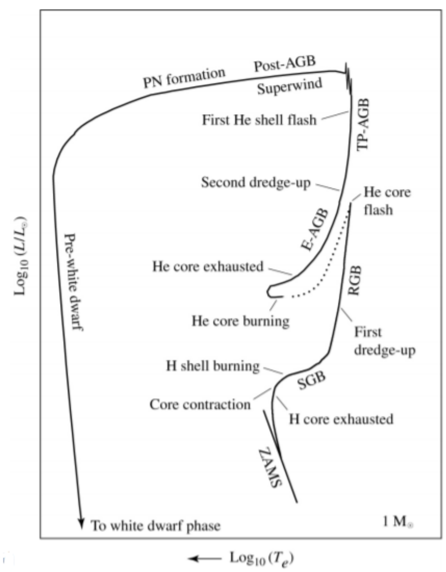

Figure 2.6: Evolution of a $1M_\odot$ star.

SGB: Sub-giant branch
RGB: Red-giant branch
AGB: Asymptotic giant branch
PN: Planetary Nebula

the core of these stars. This causes the star to contract before the shell surrounding the core is hot enough to fuse hydrogen, resulting in an increase in surface temperature, appearing as a *blue hook* on the HR diagram. The core continues its contaction under gravitational pressure, while the outer envelope rapidly expands, similar to the case in low mass stars.

The point of difference, however, arises from the fact that in high mass stars, helium core degeneracy **does not** set in before helium fusion. This, in fact, is in line with the trend that the more massive the star, the earlier helium burning sets in. This results in the observation of stars situated in the Hertzsprung Gap that have begun helium ignition before even ascending the red-giant branch. Hence, helium flashes are not observed in these stars, instead there is regular burning of helium into carbon via the triple-α process. The triple-α process releases lesser energy per unit mass than the p-p and CNO cycle, hence, the lifetime of this period is considerably shorter- roughly 10% of the main sequence lifetime.

$$
{}^{4}_{2}\mathrm{He} + {}^{4}_{2}\mathrm{He} \longrightarrow {}^{8}_{4}\mathrm{Be}
$$
$$
{}^{8}_{4}\mathrm{Be} + {}^{4}_{2}\mathrm{He} \longrightarrow {}^{12}_{6}\mathrm{C} + 2\,\gamma
$$

Once the helium in the core is exhausted, the core once again begins to contract until it becomes hot enough for helium burning to commence in a shell surrounding the core, and carbon burning commences in the core, at which point nuclear burning is now stable again. As with the case of helium burning, the lighter stars burn carbon in a degenerate core, while the more massive ones commence carbon burning before degeneracy sets in.
This pattern of fuel exhaustion, core contraction, core ignition and shell ignition continues as the star continues to fuse higher and higher elements in its core, with each successive burning period taking lesser time than the previous one. This results in the star developing a layered structure.

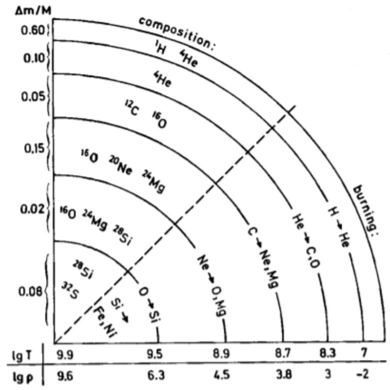

Figure 2.7: "Onion-Skin" internal structure of a $25M_{\odot}$ star.

The issue sets in when the star accumulates iron in its core. Iron being the most tightly bound nucleus, it is not possible for a nuclear reaction with iron to release energy. Hence, at this point, there is no energy source for the star, and gravitational collapse begins. But unlike previous phases, there is no subsequent energy source to balance the collapse. Thus, this is the onset of a *supernova*, which we shall cover in the next chapter. However, during this collapse, the high temperature in the core adds neutrons to iron via either the slow or *s-process*, or the rapid or *r-process*. This leads to the nucleosynthesis of higher atomic species as well as neutron-rich isotopes of these species.

Stage	Time Scale
Hydrogen	11 My
Helium	2 My
Carbon	2000 y
Neon	0.7 y
Oxygen	2.6 y
Silicon	18 d
Iron core collapse	1 s

Even while being on the main sequence, mass loss is extremely important for high mass stars. Stars as massive as $60M_{\odot}$ can lose up-to a quarter of its mass while on the main sequence. With increasing mass, radiation pressure becomes more and more important, driving away large portions of the stars mass from its weakly-held outer layers. One vivid example is that of *Eta Carinae*, a massive blue variable star of mass $\sim 100M_{\odot}$, that experiences a mass loss of $10^{-2}M_{\odot}$ year^{-1}, via a bipolar outflow.

Such mass loss results in a special class of stars known as *Wolf-Rayet stars*. These are stars that have atmospheres containing very little hydrogen. This is due to the fact that over evolution, so much mass is lost, that the entire hydrogen burning shell in the outer reaches of the star is ejected. Thus the star shows a spectrum with emission lines of helium and heavier elements, but lack those

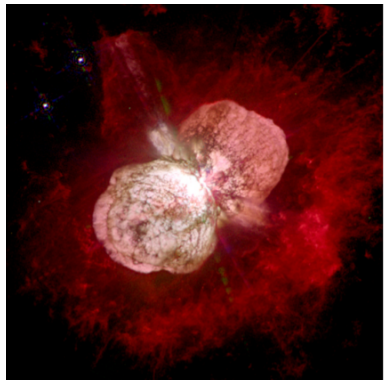

Figure 2.8: Bipolar outflow from Eta Carinae.

of hydrogen.

Mass loss is extremely important in the case of high mass stars, because of the fact that it is the final mass of the core of the star which determines whether the star explodes as a supernova, and the nature of the stellar remnant. It is interesting to notice that high mass stars evolve at roughly the same luminosity. This is due to the existence of a limit on the luminosity of a star, known as the *Eddington Luminosity.* This is the explanation behind high mass stars not having a red-giant phase, which entails an increase in luminosity.

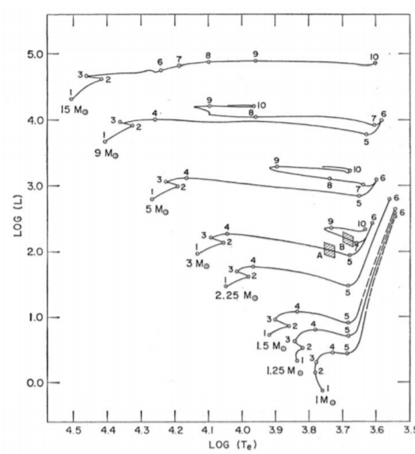

Figure 2.9: Evolution of stars of different masses.

Chapter 3

Stellar Death and Novae

In 1932, astronomers Fritz Zwicky and Walter Baade at Caltech were investigating a peculiar type of object, which was then thought to be a star, that would suddenly flare up in brightness by a factor of more than 10,000, only to dim back to normalcy within a month. Studying the observational data of each of these previous superluminous events, Zwicky arrived at the conclusion that this was produced by the explosion of a massive star. In fact, he went as far as attributing the origin of cosmic rays to these events (we now know that a significant fraction of cosmic rays originate in supernovae). Finally, in their 1934 paper, they coined the name "**supernovae**" for these events.

We now know of supernovae as extremely violent events, mainly associated with core collapse of massive stars. Huge amounts of energy are liberated at a rapid rate, as the star explodes and ejects its outer layers at a very high velocity. At its peak, supernovae can even outshine all the stars in its host galaxy for a brief period.

Figure 3.1: Supernova in NGC 2525. Supernova is to the left in the marked region.

3.1 Types of Supernovae

Supernovae are broadly classified into two types: **Type-I** and **Type-II**, depending on the presence or absence of the Balmer lines of the hydrogen spectrum (the initial lines of the Balmer series lie in the visible spectrum). These hydrogen lines are absent in Type-I supernovae, and are present in Type-II. These types are further subdivided into sub-types depending on the presence or absence of other spectral lines, and the nature of their light curves. A natural explanation for this basic difference in spectral lines can be drawn from the fact that Type-I supernovae occur in stars that have lost their hydrogen envelope, while Type-II supernovae occur in stars that still retain the hydrogen envelope.

However, there exists a compelling case to study **Type-Ia** supernovae apart from the others, due to the peculiar reason that, while the other sub-types occur due to core collapse in massive stars, Type-Ia supernovae are not attributed to such events.

3.1.1 Core-Collapse Supernovae

Let us now pick off from where we left the evolution of high mass stars in the previous chapter. The star now consists of various layers of different compositions surrounding an inert iron core. At this point, the extremely high pressure and temperature at the core mean that the core is degenerate, and the degeneracy pressure alone supports the weight of the star. As nickel burning in the surrounding shell continues to deposit iron on the core, the mass of the core grows.

Once the core reaches $1.4M_{\odot}$, the (electron) degeneracy pressure can no longer support the star, and the star begins to collapse (the figure of $1.4M_{\odot}$ corresponds to the Chandrashekhar Limit, which we shall visit in the next chapter). During the ensuing collapse, the outer part of the core can reach velocities up-to about a quarter of the speed of light. Meanwhile, in the core, high energy gamma rays are produced, which cause **photodisintegration** of iron atoms into helium nuclei and neutrons. These helium nuclei too may undergo photodisintegration. This break-up further draws away energy from the core, hastening the collapse.

$$
\begin{aligned}
{}^{56}_{26}\mathrm{Fe} + \gamma &\longrightarrow 13\,{}^{4}_{2}\mathrm{He} + 4\,\mathrm{n} \\
{}^{4}_{2}\mathrm{He} + \gamma &\longrightarrow 2\,{}^{1}_{1}\mathrm{H} + 2\,\mathrm{n}
\end{aligned}
$$

Under normal circumstances, free neutrons produced spontaneously decay into protons via β-decay:

$$\mathrm{n} \longrightarrow \mathrm{p} + \mathrm{e}^{-} + \bar{\nu_{\mathrm{e}}}$$

However, in the hot, highly dense and relativistic collapsing core, this process is no longer energetically favourable. Instead, the reverse process becomes spontaneous, and the escaping neutrinos cause an even larger loss of energy from the core:

$$\mathrm{p} + \mathrm{e}^{-} \longrightarrow \mathrm{n} + \nu_e$$

These processes lead to an enormous neutrino luminosity, much larger than $10^{15}\,L_{\odot}$. Meanwhile, the core composition becomes increasingly neutron-rich, a process known as **neutronisation**. As the core continues to collapse, the neutrons get squeezed tightly together and degeneracy starts setting in the core. But at this point, it is *neutron degeneracy pressure* which resists the gravitational pressure. The core now has densities of the order of atomic densities, and is, in essence, a giant atomic nucleus. Thus, a *neutron star* is born. In case the star is much more massive, even the neutron degeneracy pressure is unable to resist the gravitational pressure, and is overcome, causing further collapse to form a *black hole*.

The infalling matter from the outer layers rebound off the now stiff core, and propagate outwards at a substantial fraction of the speed of light. This is called **core bounce**. The outflowing gas meets the infalling gas, forming a violent, dense and extremely hot, yet stalling, shock front. About 1% of the outflowing neutrinos also gets absorbed by this front, further heating it up and re-invigorating it. The blast wave blows through the outer layers of the star, and in this process, is responsible for the formation of most of the naturally occuring heavy elements, through *explosive nucleosynthesis*.

From the outside, everything appears normal with the star, until the blast wave reaches the star's surface. After this, the star becomes a rapidly expanding ball of gas, increasing in luminosity. Over several weeks, the expanding gas begins to cool, thin and become transparent, causing to luminosity to drop. What is left behind is a stellar remnant- a corpse, that is either a neutron star or a black hole, indicating the how massive the progenitor star was at the time of its death.

The slow exponential decline in brightness can be seen by looking at the light curve for the supernova. However, there is a characteristic "bump" in the curve, where the decay slows or comes to a complete halt for a few weeks. This is attributed to the decay of radioactive isotopes of Ni and Co, which heats up the surrounding matter.

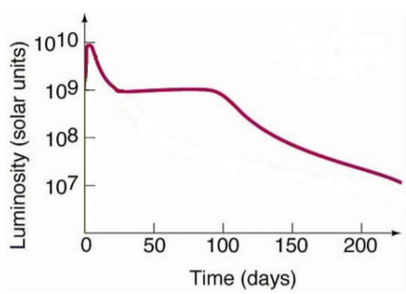

Figure 3.2: General light curve for core-collapse supernovae.

If we were to draw out an energy budget for these supernovae, we would find something very astonishing. The energy budget for a core of mass $1.5M_\odot$:

Grav. energy released	$\Delta E_{grav} = 3 \times 10^{46}$ J
Neutronisation	$\Delta E_{nuc} = 2 \times 10^{45}$ J $\sim 0.067\Delta E_{grav}$
Envelope ejection	$\Delta E_{bind} = 5 \times 10^{44}$ J $\sim 0.017\Delta E_{grav}$
KE of envelope	$\Delta E_{kin} = 1 \times 10^{44}$ J $\sim 0.003\Delta E_{grav}$
Radiation	$\Delta E_{rad} = 1 \times 10^{44}$ J $\sim 0.003\Delta E_{grav}$
Total	$\sim 0.09\Delta E_{grav}$

We can see that only about $\sim 1\%$ of the gravitational energy released by the dying star is involved in the explosion. And even after taking into consideration neutronisation, photodisintegration and envelope ejection, a considerable amount of energy is left unaccounted for. This energy deficit, is radiated away in the form of neutrinos, formed in the collapsing core. These neutrinos do not escape immediately, but eventually escape carrying away a bulk of the energy with them.

3.1.2 Type-Ia Supernovae

Type-Ia supernovae do not possess the bump that was characteristic to core collapse supernovae on their light curves. All properties of these supernovae, point towards a thermonuclear origin- these supernovae result from the collapse of a white dwarf in binary star systems. These kinds of supernovae are extremely rare, occurring less frequently than other kinds of supernovae.

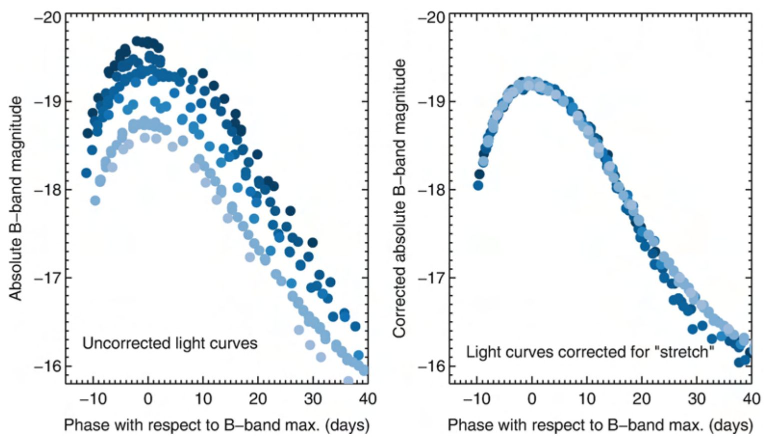

Figure 3.3: Light curve for Type-Ia supernovae.

While the light curves of different Type-Ia supernovae peak at different values, on applying a "stretch factor" correction to them, based on taking into consideration color and magnitude of the progenitor, the light curves become remarkably homogeneous. This allows us to use Type-Ia supernovae as **standard candles-** sources with a known luminosity, using which we can calculate cosmic distances. Another example of standard candles used by astronomers are a special kind of star known as *Cepheid variable stars*. These stars undergo a variation in luminosity over a regular cycle, the period of which is closely linked with the luminosity.

These supernovae generally occur when a white dwarf accretes matter from its companion star in the binary system, causing the mass of the white dwarf to approach the Chandrashekhar limit. If it manages to accrete enough matter to push its mass over the limit, the electron degeneracy pressure supporting it would give away causing further collapse to a neutron star. However, it is believed that as the white dwarf comes close to the Chandrashekhar limit, ignition temperature of the carbon constituting it is achieved, causing a widespread nuclear runaway reaction (due to the degenerate nature of the dwarf), thereby causing a supernova explosion. Since the mass around which this explosion takes place is the same, the light curves for Type-Ia supernovae are similar. However, the exact conditions of the runaway reaction, as well as the nature of the progenitor (merger of two white dwarfs or white dwarf accreting matter from neighbour) are still under speculation.

3.2 A Case Study: SN1987A

On 23$^{\mathrm{rd}}$ of February 1987, a supernova was detected in the Large Magellanic Cloud, a satellite galaxy of the Milky Way. At 168,000 light years, this was the closest detected supernova to Earth since Kepler's Nova (which was Type-Ia) in 1604. Since it was the first supernova that astronomers were able to study in great detail, it was one of the most exciting astronomical events of the time.

The first detection of the supernova was actually a neutrino detection, due to the fact that neutrino emission takes place before visible light is emitted. The Kamiokande-II experiment in Japan and the IMB experiment in Ohio detected 12 and 8 neutrinos respectively. The two detectors detected the neutrinos almost simultaneously, in a burst lasting 12 seconds.

About 3 hours after the neutrino detection, the first visible light observations were made, viewed independently by atleast 4 different observers. Initial observations tentatively established the progenitor star to be Sk-69° 202. The obtained light curve is consistent with what is expected of a core collapse supernova. Furthermore, several satellites detected γ-ray emission lines from $^{56}_{27}$Co, which was proof that radioactive cobalt was produced in the supernova explosion.

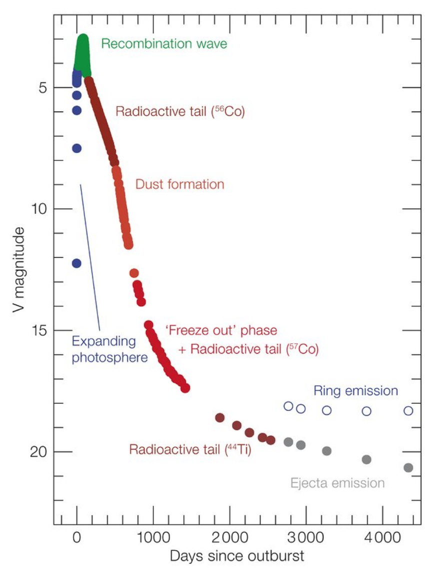

Figure 3.4: Light curve of SN1987A.

Later visual observations indicated that the progenitor star had disappeared, clinching proof for a supernova explosion. Also observed, was a system of three rings of glowing gas- an inner ring and two outer rings on either side of the equatorial plane. The formation of these rings is an indicator for violent mass loss- fuelling speculations that the supernova may have occurred due to accretion of matter from a companion star.

Based on the mass of the initial star and neutrino emission data, it is expected that the stellar remnant is a neutron star. However, intensive searching has not yet yielded an observation of the remnant. Evidence presented in 2019 suggests that the remnant is enshrouded inside the brightest clumps of dust. In 2021 measurements of X-Rays emitted suggest that they originated from a neutron star.

Figure 3.5: Remnant of SN1987A.

Chapter 4

White Dwarfs

When low mass stars reach the end of their evolution, the stellar remnant they leave behind is a white dwarf, which are the most common stellar remnant ($\sim$ 97% of evolved stars). These are extremely dense objects consisting of electron-degenerate matter. Wit no nuclear fuel remaining, these objects lack an energy source to support themselves against gravity.

The first white dwarf discovered was Sirius B, the dim companion star of Sirius A, both of which constitute the binary star system of Sirius, the brightest star in the night sky. With a mass of $1.02M_\odot$ and a volume roughly that of the Earth, it has a mean density $\rho \sim 10^9$ kg m^{-3}. It was also the source of great controversy in the 1920s, as physicists failed to conceive of a mechanism for its internal support. A resolution was finally provided in 1926 by R.H. Fowler who suggested that they are supported by *degeneracy pressure*, and Chandrashekhar who expanded on his work.

4.1 Degeneracy Pressure

At the high densities which are prevalent in white dwarfs, gas particles are so close to each other that the interactions between them have to be taken into account. At this point, it is important to consider **Pauli's Exclusion Principle**, which states that two or more identical fermions can not occupy the same quantum state. In other words, a single quantum state can be occupied by just two electrons of opposite spin. The volume of each quantum state in phase space is given by h^3, where h is Planck's Constant.

As the pressure (and density) in the white dwarf increases, electrons become confined to a smaller phase-space, with electrons of opposite spin occupying the same state. Eventually, all the lower energy states fill up first upto a particular state.

Let us consider a perfectly degenerate gas of electrons, with all quantum states upto a momentum p_F (called Fermi momentum) occupied. Thus, no higher states with momentum greater than p_F are occupied.

The volume of momentum-space occupied by electrons with momenta in the range p to $p + \mathrm{d}p$ corresponds to the volume of a spherical shell with radius p and thickness $\mathrm{d}p$, given by $4\pi p^2 \, dp$.

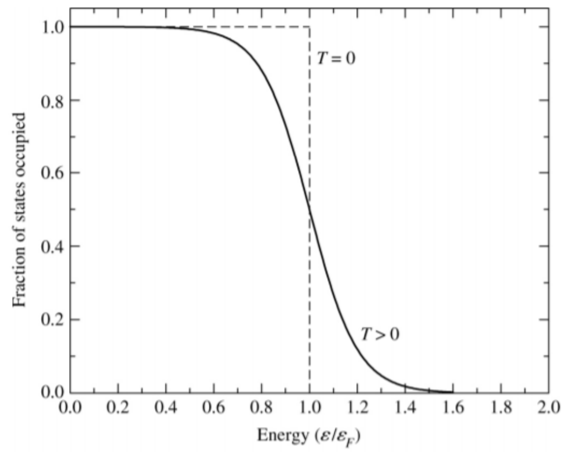

Figure 4.1: Energy states occupied. $T = 0$ corresponds to a perfectly degenerate gas.

Since the volume of each quantum state is given by h^3, and the number of electrons that can occupy a quantum state is 2, the number of quantum states per unit volume with momenta in range p to $p + \mathrm{d}p$ is given by

$$n_e(p)\,dp = \begin{cases} \dfrac{2}{h^3} 4\pi p^2\,dp & p \leq p_F \\ \\ 0 & p \geq p_F \end{cases}$$

Hence, the total number of electrons per unit volume is obtained by integrating the above expression over all momenta

$$n_e = \int_0^\infty n_e(p)\,dp = \frac{8\pi}{h^3}\int_0^{p_F} p^2\,dp = \frac{8\pi {p_F}^3}{3h^3}$$

Rearranging, we obtain the maximum momentum, otherwise known as Fermi momentum

$$p_F = \left(\frac{3h^3 n_e}{8\pi}\right)^{1/3} \tag{4.1}$$

We can now obtain the pressure of the degenerate gas as

$$\begin{aligned} P &= \frac{1}{3}\int_0^\infty v\,p\,n_e(p)\,dp \\ &= \frac{1}{3}\int_0^{p_F}\left(\frac{p}{m_e}\right) p\,\frac{2}{h^3} 4\pi p^2\,dp \end{aligned}$$

where v is velocity of the electrons possessing momentum p. Hence degenerate pressure is given by

$$P_{deg} = \frac{8\pi}{15 m_e h^3} {p_F}^5 = \frac{h^2}{20 m_e} \left(\frac{3}{\pi}\right)^{2/3} {n_e}^{5/3} \tag{4.2}$$

However, this expression only holds for a non-relativistic scenario. If we were to proceed with a relativistic treatment, i.e. $p \gg m_e c$, we would arrive at

$$P_{deg} = \frac{hc}{8} \left(\frac{3}{\pi}\right)^{1/3} {n_e}^{4/3} \tag{4.3}$$

It is more useful to obtain an equation of state for a white dwarf, by deriving an expression relating the pressure with its density. For this, we have to first relate the electron density with the density. For every hydrogen atom of mass m_H, there is one electron, and for higher elements, there is one electron for every $2m_H$ mass. Thus,

$$n_e = \frac{\rho X}{m_H} + \frac{\rho\,(1 - X)}{2m_H} = \frac{\rho\,(1 + X)}{2m_H} \tag{4.4}$$

where X is the hydrogen fraction. Now, we can express our results in a compact form,

$$P_{deg} = \kappa \rho^{\gamma} \tag{4.5}$$

where, in a non-relativistic case,

$$\kappa = \frac{h^2}{20 m_e} \left(\frac{3}{\pi}\right)^{2/3} \left(\frac{1 + X}{2m_H}\right)^{5/3} \quad \text{and} \quad \gamma = 5/3$$

and in a relativistic case,

$$\kappa = \frac{hc}{8} \left(\frac{3}{\pi}\right)^{1/3} \left(\frac{1 + X}{2m_H}\right)^{4/3} \quad \text{and} \quad \gamma = 4/3$$

As we can see, the degeneracy pressure is independent of temperature, and only depends on density and chemical composition. The condition of degeneracy, however, depends on density and temperature. It is important to consider degeneracy for "cold" gases, wherein Fermi momentum is much larger than classical momentum. Note that these "cold" gases can actually have high temperatures. In stars with degeneracy, there is no sharp transition between regions of degenerate and non-degenerate gas- the transition is smooth. The solution in the case of partial degeneracy requires a more complex solution. Similarly, the transition of regions of ideal gas behaviour and electron degenerate behaviour is smooth.

As the mass of the white dwarf increases, the pressure and the density keep increasing, and the electron gas becomes more and more relativistic. This would mean that there might exist a limiting case on the mass of a white dwarf. Hence, it would make sense to probe for such a limit while considering the electrons in the star to be purely relativistic, i.e. the white dwarf has an equation of state of form equation (4.5) with $\gamma = 4/3$.

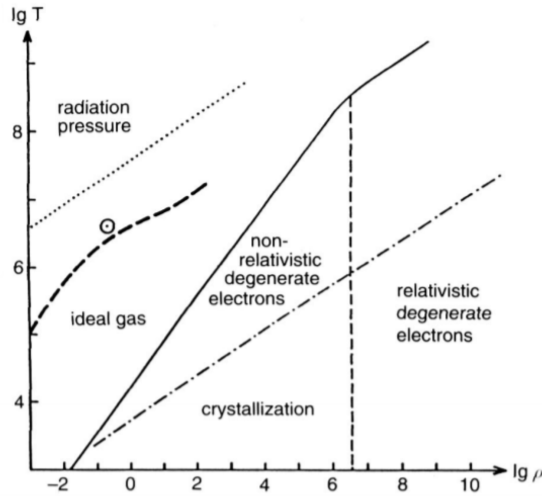

Figure 4.2: Density-Temperature plot showing regions where different equations of state are applicable. Heavy dashed line shows location of Sun.

4.2 Chandrashekhar Limit

From the first two equations of stellar structure, equations (2.3) and (2.5), we can find a second-order differential equation between pressure p and density ρ by eliminating mass M between these equations

$$\frac{d}{dr}\left(\frac{r^2}{\rho}\frac{dp}{dr}\right) + 4\pi G\rho r^2 = 0 \tag{4.6}$$

Now, we know that the equation of state for a white dwarf is given by $p = \kappa\rho^\gamma$. Such solutions are known as *polytropes*, and are usually written in terms of the *polytropic index* n, given by $\gamma = 1+n^{-1}$. Thus, in a non-relativistic case, $\gamma = 5/3$ and $n = 3/2$, while in a relativistic case, $\gamma = 4/3$ and $n = 3$. Using a complex change in variables, we can reduce equation (4.6) to a more manageable form. First, we write distance from centre $r = a\xi$ and density $\rho = \rho_c\theta^n$, where θ is a function of the dimensionless distance ξ, n is the polytropic index, and ρ_c is the density at the centre of the white dwarf. Taking

$$a = \left[\frac{(n+1)\kappa{\rho_c}^{(1/n)-1}}{4\pi G}\right]^{1/2}$$

the differential equation takes that form

$$\frac{1}{\xi^2}\frac{d}{d\xi}\left(\xi^2\frac{d\theta}{d\xi}\right) + \theta^n = 0 \tag{4.7}$$

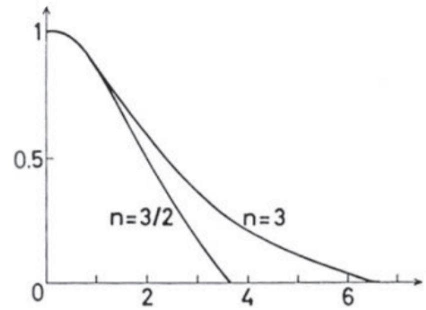

Figure 4.3: Solutions of Lane-Emden equation for polytopes $n = 3/2$ and $n = 3$. Vertical axis represents θ and horizontal axis represents ξ.

This is the famous **Lane-Emden Equation**, a dimensionless form of Poisson's equation for a Newtonian, self-gravitating, spherically symmetric fluid. The equation is difficult to solve, and analytic solutions for $\theta_n(\xi)$ only exist for $n = 0, 1$ and 5. However, numerical solutions do exist for other values of n. For all values of n under 5, the density goes to zero at a finite radius ξ_n, corresponding to the surface of the star at radius $R = a\xi_n$.

In order to obtain mass-radius relationship, we integrate the density distribution from $r = 0$ to R

$$\begin{aligned} M &= \int_0^R 4\pi r^2 \rho\, dr = 4\pi\rho_c \int_0^R \theta^n r^2\, dr \\ &= 4\pi\rho_c a^3 \int_0^{\xi_n} \theta^n \xi^2\, d\xi = 4\pi\rho_c \left(\frac{R}{\xi_n}\right)^3 \int_0^{\xi_n} \theta^n \xi^2\, d\xi \end{aligned} \tag{4.8}$$

However, from equation (4.7), we can see that

$$\int_0^{\xi_n} \theta^n \xi^2\, d\xi = -\left(\xi^2 \frac{d\theta}{d\xi}\right)_R$$

Therefore, we get

$$M = 4\pi\rho_c \left(\frac{R}{\xi_n}\right)^3 \left[-\xi^2 \frac{d\theta}{d\xi}\right]_R \tag{4.9}$$

It is interesting to note that $M \propto \rho_c R^3$. Furthermore, from the definition of a, we can see that $\rho_c \propto R^{2n/(1-n)}$. Putting these together, we arrive at $M \propto R^{(3-n)/(1-n)}$. For the polytrope $n = 3/2$ (non-relativistic), we see that $M \propto R^{-3}$, i.e. more massive white dwarfs are *smaller*. Consequently, for a degenerate, relativistic white dwarf ($n = 3$), mass is independent of radius.

For the polytrope $n = 3$, the numerical figures quoted by Kippenhahn and Weigert for the quantity in square brackets in equation (4.9) is 2.01824 (similarly for $n = 3/2$ it is 2.71406). So, computing the mass of a relativistic, degenerate star,

$$M = 2.01824 \times 4\pi\rho_c \left[\frac{\kappa {\rho_c}^{-2/3}}{\pi G}\right]^{3/2}$$

after using the expression for a. Substituting the value for κ and simplifying the expression,

$$M = 5.699 \left(\frac{1+X}{2}\right)^2 M_\odot \tag{4.10}$$

For a white dwarf, which is predominantly a He or CO core, hydrogen fraction $X \approx 0$. Finally, this gives us

$$M_{Ch} = 1.44 M_\odot \tag{4.11}$$

This is the **Chandrashekhar limit**, a limit on the mass of a white dwarf capable of supporting itself by electron degeneracy pressure, and was derived by Subrahmanyan Chandrasekhar in 1930. It only depends on fundamental constants and is the *unique* mass a purely relativistic white dwarf can possess (as real white dwarfs are partially relativistic). The distribution of masses of white dwarfs, however, is strongly peaked at $M \sim 0.6 M_\odot$, with the most massive known white dwarf being $1.35 M_\odot$.

The implications of Chandrashekhar's work caused ripples in the world of astrophysics at the time. In particular, the role of the 4/3 ($\gamma = 4/3$) resistance in the relativistic domain. From Figure 4.4 it is clear that as stellar objects with masses under $1.4 M_\odot$ undergo contraction due to gravity, they meet the 5/3 resistance solid line at higher circumferences and the 4/3 resistance solid line at lower circumferences (remember, massive white dwarfs are smaller). If they meet the resistance line, they settle there and remain stable.

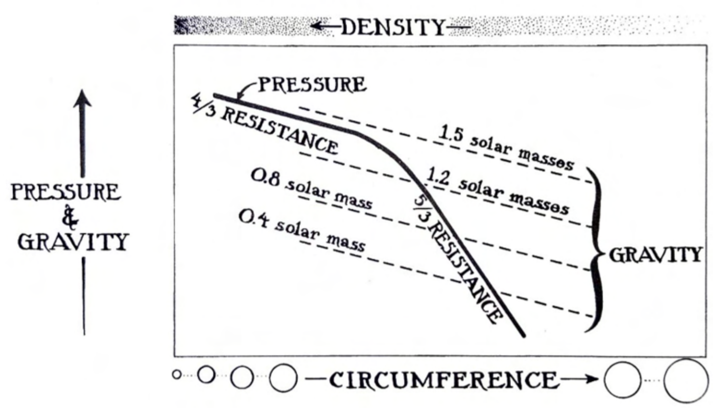

Figure 4.4: Plot showing white dwarf resistance to compression.

However, if the object has mass greater than $1.4 M_\odot$, it moves parallel to the 4/3 resistance line and continues contraction. This would mean that even electron degeneracy pressure would be insufficient to resist collapse, possibly collapsing into a black hole. This hinted towards the existence of black holes, which were already discovered as a solution of Einstein's field equations, but were an anathema to most of the world's astrophysicists, including Arthur Eddington, who also happened to be Chandrashekhar's advisor. Such was the gravity of the situation, that Eddington proposed modifying relativistic mechanics in order to keep the polytrope with $n = 5/3$ universally applicable. Eddington's stature and his opinion over the Chandrahekhar limit, was in large part, responsible for Chandrashekhar winning the Nobel Prize for his work only about half a century later.

4.3 Fate and White Dwarf Cooling

White dwarfs in a stellar neighbourhood may either accrete matter from a neighbouring star or merge with another white dwarf, causing a Type-Ia supernova, or they may get consumed themselves by an even more massive star. However, in the absence of such scenarios, the fate of a white dwarf is simple- cooling.

Due to the absence of any internal nuclear reactions, a white dwarf continues cooling, radiating its internal thermal energy. Conduction of heat by degenerate electrons is so efficient that the interior of a white dwarf is nearly isothermal, with temperature dropping significantly only at the surrounding thin ($\sim 1\%$ of radius) non-degenerate layer. The steep temperature across this layer causes it to be convective, acting as an insulating blanket, slowing down the leakage of energy. Even after considering an unrealistically efficient cooling mechanism, it takes roughly 10^9 years for a newly formed white dwarf of mass $1M_\odot$ to cool to about 10^3 K. There exist white dwarfs *12 billion years* old that still have a surface temperature of about 3800 K.

Furthermore, as the white dwarf continues cooling, it gradually crystallises from the centre outwards. The developing crystal structure minimizes the vibrational energy of electrons. The phase change that occurs further slows down cooling. The white dwarf thus continues to radiate away its thermal energy, and since its radius remains constant, it follows a linear path along the HR diagram towards the bottom-right - the **white dwarf cooling track**. The white dwarf finally ends its long luminous life after radiating all its energy, as an invisible *black dwarf.* However, the universe is still too young to be able to have formed these objects, due to the slow nature of the cooling track.

Chapter 5

Neutron Stars

When Zwicky and Baade were struggling with the problem of supernovae (see chapter 3), the discovery of the neutron had just arrived on the scene. Fascinated by the neutron, Zwicky was convinced that it was the missing piece to the supernova puzzle. He reasoned that if a star were to contract upto certain high densities, the stellar core would become a "gas" of neutrons - he called it a *neutron star*. The formed neutron star would not only be extremely small, but would be only a small fraction of the original star's mass. He believed that this loss in mass was key to providing the tremendous energy output of a supernova.

While their theory about supernovae was responded to with enthusiasm by the scientific community, the neutron star theory was termed as "too speculative", and fizzled out. However the idea finally caught the eye of scientists when renowned Soviet physicist Lev Landau published a similar paper on "neutron cores" - this paper was actually a last-ditch attempt by Landau to escape arrests from the Soviet government. The idea caught the eye of Robert Oppenheimer and his students, who worked on this problem.

We now know that neutron stars are extremely dense objects, with masses greater than that of the Sun, but only as large as a city, and their surrounding environment is extremely violent.

5.1 Tolman–Oppenheimer–Volkoff Limit

The base conditions for stability in a neutron star are similar to that in a white dwarf- degeneracy pressure supporting the star against gravitational contraction. Since both neutrons and electrons are fermions, it would make sense to approach the problem for limiting mass of a neutron star in a way similar to Chandrashekhar's approach for white dwarfs, just replacing terms corresponding to electrons with those corresponding to neutrons. However, we must also take note of the fact that the formation of a neutron star involves the process of *neutronisation*. This can be taken into account by putting hydrogen fraction X as 1 instead of 0 (however, there is no *physical* meaning to hydrogen fraction in this case) in equation (4.10), giving us

$$M_{limit} = 5.699 M_{\odot}$$

This, however, is a serious overestimate for the limiting mass of a neutron star. This is because we have ignored rotational effects, proper implications of general relativity, and most importantly, the effect of strong nuclear force between neutrons. In 1939, Robert Oppenheimer and George Volkoff, using the work of Richard Tolman, obtained the limit on the mass of a neutron star sue to neutron degeneracy alone as $0.7M_\odot$, which is lower than the Chandrashekhar limit. This is due to the fact that they neglected the strong nuclear force, which was not very well understood at the time.

Further theoretical work has placed the limiting mass between $2.2M_\odot$ and $2.9M_\odot$ (in general, $\leq 3M_\odot$), with the most massive neutron star discovered having a mass more than $2.7M_\odot$. The fact that there is not much clarity on the exact value of the Tolman–Oppenheimer–Volkoff Limit, which is analogous to the Chandrashekhar limit for white dwarfs, is a testament to how complex the physics of neutron stars is. However, the undeniable existence of the upper limit was a confirmation that unless massive stars lose enough matter to settle with a white dwarf or neutron star death, they will collapse into a black hole.

5.2 Structure

Due the small size of neutron stars which posses a considerable mass, the density in the interior $\rho \sim 10^{17}$–10^{18} kg m^{-3}, which is of the scale of nuclear densities. To give a physical feel of the tremendous densities, a teaspoon of neutron star matter would weigh as much as Mt. Everest. In fact, a neutron star can be thought of as to be a giant atomic nucleus of mass number $A \approx 10^{57}$ - it behaves as a macroscopic quantum object. The internal structures of neutron stars are not well determined because of uncertainties in the equation of state of degenerate nuclear matter, but recent models have been drawn up based on detailed physics of the interior.

The various zones in the model are:

- The crust is a solid region consisting of matter similar to what is found in crystallized white dwarfs, heavy nuclei forming a lattice embedded in a degenerate gas of electrons, as well as heavy nuclei polymers arranged cylindrically due to the strong surface magnetic field.
- A region of superfluid neutrons and degenerate electron gas. The superfluidity observed here is similar to that observed in ${}^4_3$He, wherein the helium atoms, which are fermions, exhibit superfluidity by pairing up to form *Cooper Pairs* at high densities or low temperatures. Interestingly, the problem of superfluidity was solved by Landau after his release from arrest that he was trying to avoid by publishing his paper on neutron cores.
- An inner region of superfluid neutrons and superconducting protons- the neutron liquid region. The superconductivity of the interior regions ensure that the magnetic fields do not diffuse within it, thereby "freezing" the magnetic field in place. This will have a profound impact as seen in the next section.
- The innermost core region is believed to consist of *exotic* matter quite different from neutron liquid, like a neutron solid or quark matter, due to the extremely high densities. Many neutron star models do not posses this region, but it is a possibility.

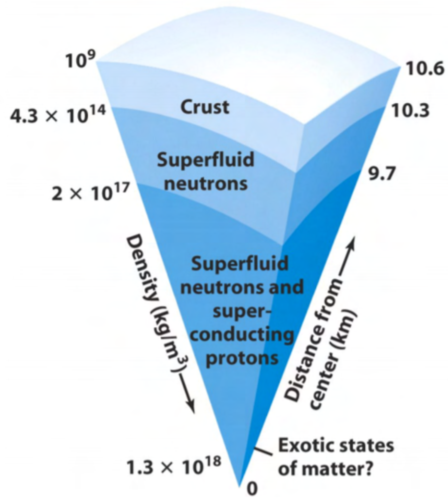

Figure 5.1: Modelled interior structure of a $1.4M_\odot$ neutron star.

5.3 Rotation and Magnetic Field

As the slowly rotating progenitor star evolves into a neutron star, it undergoes tremendous contraction. A neutron star of mass about $1M_\odot$ can have radii of the order 10 km. Applying the **law of conservation of angular momentum** here, even after taking into account mass loss, the formed neutron star spins rapidly. Neutron stars can spin at several hundred times a second, sometimes as rapidly as *1000 times* per second.

As seen earlier, the superconducting nature of the inner regions of the neutron star ensures “flux freezing” - the same magnetic flux threading the surface of the stellar core of the progenitor. Therefore, applying conservation of magnetic flux.

$$R_i{}^2 B_i = R_f{}^2 B_f \implies B_f = \left(\frac{R_i}{R_f}\right)^2 B_i \tag{5.1}$$

Taking general values of initial radius of the core as 10^4 km and final radius of neutron star as 10 km, we see that the magnetic field is boosted by a factor of 10^6. Typical value of initial magnetic field is $\sim 10^5$ gauss, thereby giving us the final magnetic field as 10^{11}–10^{12} gauss. The strongest neutron star fields reach 10^{15} gauss, but 10^{12} gauss is more typical. In perspective, the value of the Earth’s magnetic field is 0.6 gauss.

5.4 Pulsars

The first discovery of a pulsar was in 1967 by Anthony Hewish and Jocelyn Bell. The discovery though, was by accident. They were observing interplanetary scintillation by small radio sources using a new radio telescope in Cambridge, when they observed an invisible object in the sky emitting sharp radio pulses. What was even more intriguing was the fact that the pulses were at exactly equally space intervals of time, the spacing between the pulses being 1.337 s.

If a rotating body is to remain stable, the centrifugal force at the surface should balance the gravitational force. Equating the two forces,

$$m\omega^2 r = \frac{GMm}{r^2} \tag{5.2}$$

Using the relation $\omega = \dfrac{2\pi}{P}$ and rearranging, we get

$$r = \sqrt[3]{\frac{GMP^2}{4\pi^2}} \tag{5.3}$$

For an object with period 1.337 seconds, the radius comes out to be smaller than that of a white dwarf. Hence, the possible origin of these pulses must be a small, compact source- the most viable candidate being a neutron star.

5.4.1 Rotating Neutron Star Model

An interesting nature of neutron stars is the fact that the axis of the magnetic field is **not** aligned to the rotational axis- they lie askew. The sweeping, strong magnetic field acts as a dynamo, generating large electric fields near the surface. These electric fields generate ionised particles (electron-positron pairs) from the surface, which radiate away electromagnetically along the magnetic field. This results in a beam of energy originating from the magnetic poles, being swung around as the magnetic axis rotates about the neutron star spin axis - causing the neutron star to behave like a lighthouse beacon.

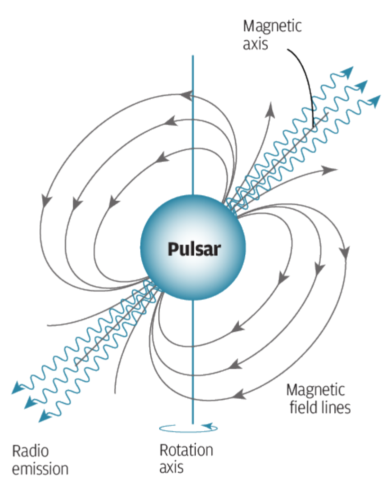

Figure 5.2: Magnetised rotating neutron star model of pulsar.

Observations made over the years have revealed that the period of rotation of pulsars actually *increases* over time. This is due to the fact that the electromagnetic energy radiated by the pulsar comes at the cost of its rotational energy. This rate of loss of rotational energy can be properly described using the *braking index* n which is defined by the relation $\dot{\omega} = -\kappa\,\omega^n$ (following the time derivative notation). The observation of rate of increase of pulsar periods has been a significant contribution towards the rotating neutron star theory. Often pulsars are plotted on a P–$\dot{P}$ plot, which can be considered to be an analogue of the HR diagram for pulsars. If we were to calculate the rate of change of rotational energy for a neutron star,

$$\frac{dE_{rot}}{dt} = \frac{d}{dt}\left(\frac{1}{2}I\omega^2\right) \tag{5.4}$$

Using the relation between angular velocity and period, we arrive at

$$\frac{dE_{rot}}{dt} = -4\pi^2 I\frac{\dot{P}}{P^3} \tag{5.5}$$

In 1054 AD, Chinese astronomers observed a new "guest star" in the sky, which was brighter than any other star in the sky, and lasted for a month before fading. Similar observations were made by other astronomers around the world. The incident that they observed was a core collapse supernova, and observations place the object that they observed in the now-known Crab Nebula, which comprises of the ejected material of the progenitor star. At the centre of the nebula is the Crab pulsar, the supernova remnant. Observation have been carried out on the Crab pulsar and the observed slowdown is

$$\frac{\dot{P}}{P} \approx 4.38 \times 10^{-13}\ \mathrm{s}^{-1}$$

Therefore, the energy generated by rotational slowdown of the Crab pulsar comes out to be

$$\frac{dE_{rot}}{dt} \approx 6.4 \times 10^{31}\ \mathrm{W}$$

Coincidentally, this is also the observed energy radiated by the Crab nebula at all wavelengths. This was vital proof for the fact that the Crab pulsar is indeed a rotating neutron star, and supports the theory in general. Unfortunately, the direct observational verification of this theory has only been successfully applied to the Crab Nebula. However, further theoretical studies have cemented the theory explaining the origin of pulsars.

Due to their huge moments of inertia, pulse periods of pulsars are extremely stable, even after taking into account their slowdown, and are as steady as atomic clocks. However, occasionally there are sudden discontinuous changes in the slowdown of the period. The larger of these discontinuous changes are termed as **glitches**. One of the mechanisms though of to produce these glitches are sudden large scale deformities in the crust of the neutron star, termed as *starquakes*, similar to earthquakes on Earth. Modern models take into account the properties of the rotating superfluid in the neutron star, and the effect of vortices in the fluid on the rotation. While the Crab pulsar has undergone glitches at an average rate of once every 4 years, the Vela pulsar glitches frequently at an observed rate of once every 2.5 years.

5.4.2 Millisecond Pulsars

Millisecond pulsars are pulsars having extremely short periods - of the order of a few milliseconds. Until the discovery of these pulsars, the Crab Nebula pulsar had the shortest known period, which was attributed to the fact that it was still relatively young. The fact that millisecond pulsars are found predominantly in globular clusters of stars provides a natural explanation for it's short period.

Being in globular clusters provides a greater probability of these objects having a companion star, i.e. they comprise a binary system. Often when the matter of the companion star comes too close to the rotating neutron star, otherwise known as crossing the **Roche Limit**, it starts falling towards the neutron star and accreting in a rotating accretion disc around it. The rotating disc transfers angular momentum to the pulsar, thereby speeding it up and allowing for smaller pulse periods. If the companion star explodes, the system can leave behind an isolated millisecond pulsar. They have weaker magnetic fields, which allows for extremely stable periods, as well as a higher spin-up rate due to the accretion disc.

5.4.3 Binary Pulsars

It was largely believed that most pulsars existed as solitary objects, with the handful of binary systems consisting of a pulsar and a star. However, in 1975, the binary pulsar PSR B1913+16 was discovered. Based on observations, the period of the binary system was determined to be 7.75 hours, which was remarkably short. This led to conclusions that both the component objects of the binary system were massive, probably neutron stars.

Being a relativistic binary, this was the first accurate determination of neutron star masses, using the effect of time dilation due to the two gravitating objects on the Doppler shift. The masses of both neutron stars was determined to be roughly equal to $1.4M_{\odot}$. Furthermore, it was determined that only one of the neutron stars was a pulsar. The system also provided an environment for extremely sensitive tests of general relativity. One of the most significant outcomes was the measurement of orbital decay of the system exactly matched predictions of general relativity. It predicts that the system's orbital energy is radiated away in the form of gravitational waves, which can be detected by gravitational wave observatories such as LIGO.

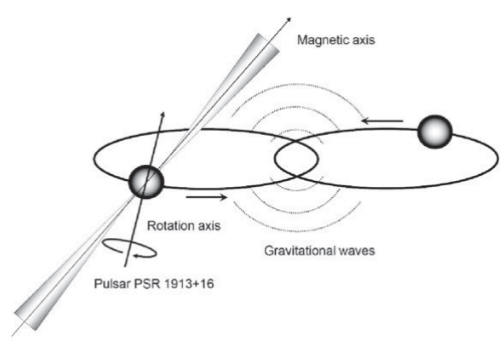

Figure 5.3: Model of PSR B1913+16 binary system.

Chapter 6

Black Holes

The concept of a black hole was actually first thought up in 1783, by John Michell. At the time Newton's corpuscular or particle theory of light was widely prevalent among the scientific community. Having accepted this theory, Michell devised of a scenario where light particles emanating from the surface of a star are unable to escape the gravitational pull and fall back to the surface, much like throwing a projectile on Earth with a speed less than the escape speed. Michell noted that such a "dark star" would not be visible at distances beyond the maximum point of the light particles' path, and we would have no information regarding such bodies apart from what could be inferred from the motion of other luminous objects around it. This theory was further propounded by French mathematican Pierre-Simon Laplace. However, Michell's extremely accurate predictions were so far ahead of it's time that it made very little impression of the contemporaries of his time, and the theory faded in obscurity.

While the Schwarzschild solution to Einstein's field equations which described a black hole existed since 1916, the idea of a black hole existing in the real Universe was shunned by many scientists. But this started to change after it was confirmed that implosion of stars with a final mass of more than $3M_\odot$ was necessary, and the star could not halt at the white dwarf or neutron star stages. Oppenheimer and his student Hartland Snyder ran computations for the collapse of an ideal, spherical, imploding star and the revelations were shocking. The computations suggested that as viewed by an external static observer, the imploding star would appear to freeze at the critical radius, while an observer riding the star's implosion would see the implosion continuing past the critical radius.

The seemingly paradoxical predictions of the Oppenheimer-Snyder calculations were seen as a result of the idealisation and provoked wide skepticism, however later theoretical insights by David Finkelstein in 1958 appeared to clear up the situation and the scientific community began to grow more accepting towards the theory.

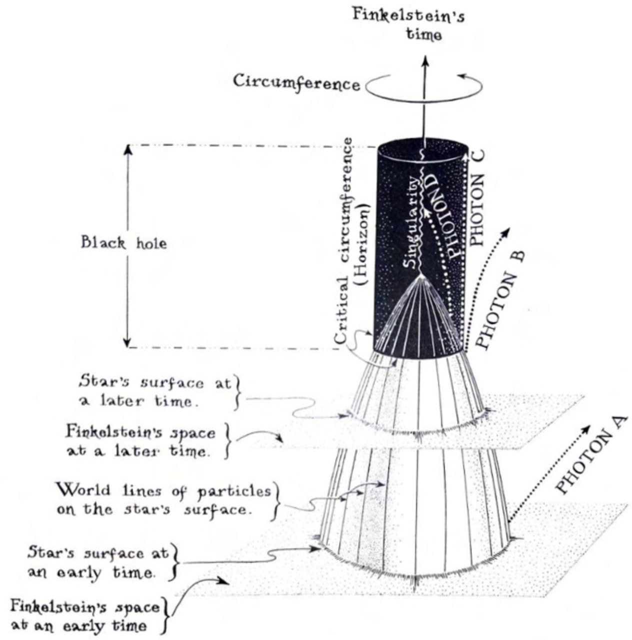

Figure 6.1: A space-time diagram showing Finkelstein's insight into the Oppenheimer-Snyder collapse. The horizontal plane shows the 2D space cross-sections of the imploding star, and plotted vertically is increasing time. Worldlines are paths followed by particles on space-time diagrams. As can be seen, photons A and B emitted prior to the formation of the hole propagate outwards, photon C emitted at the formation of the hole stays at the horizon, and photon D emitted after hole formation never escapes.

6.1 Solutions to Einstein's Field Equations

There exist four key solutions of Einstein's field equation that describe black holes: Schwarzschild metric (uncharged, non-rotating), Kerr metric (uncharged, rotating), Reissner-Nordström metric (charged, non-rotating) and Kerr-Newman metric (charged, rotating), of which we shall briefly cover the first two key solutions.

6.1.1 Schwarzschild Metric

The Schwarzschild metric is an exact solution to Einstein's field equations that was derived in 1916 by Karl Schwarzschild. It describes the gravitational field in the vicinity of a spherical black hole that is non-rotating and uncharged. Let us first approach this from a Newtonian perspective.

The velocity of projection required for a mass to escape that gravitational influence of an object, otherwise known as *escape velocity*, is given by,

$$v_e = \sqrt{\frac{2GM}{r}} \tag{6.1}$$

The critical radius of a black hole is obtained when this escape velocity becomes equal to the speed of light, as for smaller radii, even light would be unable to escape the gravitational field. This critical radius is known as the **Schwarzschild radius** and is given by,

$$r_s = \frac{2GM}{c^2} = 2.95\frac{M}{M_\odot}\ \text{km} \tag{6.2}$$

Surprisingly the obtained radius after proceeding through a classical treatment is exactly the same as what was obtained by Schwarzschild through a relativistic treatment, which follows from

$$\nu_\infty = \nu_{em}\left(1 - \frac{2GM}{rc^2}\right)^{1/2} \tag{6.3}$$

As we can see, any electromagnetic wave emitted from $r = r_s$ is redshifted (frequency is shifted towards red-end of spectrum, i.e. to lower frequencies) to zero frequency, and any wave emitted at smaller radii no longer "exists". The surface at this critical radius is termed as the **event horizon**. Another important result is the existence of a *last stable circular orbit* at $r = 3r_s$. Any circular orbit within this radius will be unstable and the orbiting objects would spiral into the hole. The binding energy for this last stable orbit is given by

$$\left[1 - \sqrt{\frac{8}{9}}\right] = 0.0572$$

or 5.72% of the rest-mass energy of that orbit.

At the center of the black hole lies the **singularity**, a region where density and gravitational field (or curvature) is infinite according to the solution to general relativity. In the case of Schwarzschild black holes, the singularity is a point and has zero volume, and can be thought of to contain all the mass of the black hole which imploded to the point. The appearance of singularities in general relativity is commonly perceived as signaling the breakdown of the theory, and occurs in situations where quantum effects should come into play in describing the behaviour of particles. Therefore there are ongoing attempts to mesh the laws of gravity and quantum mechanics - a law of *quantum gravity*, which is expected not to feature any singularities.

6.1.2 Kerr Metric

The Kerr metric was discovered by mathematician Roy Kerr in 1963. At first, it was thought that it was a special solution that described the gravitational field near a spinning star, but it was soon realised that it was a general description of the space-time geometry in the vicinity of any spinning black hole. Rotating black holes, also known as Kerr black holes, possess a number of properties that make it of utmost relevance in high energy astrophysics, as well as the most challenging, due to the complexity of the mathematics involved.

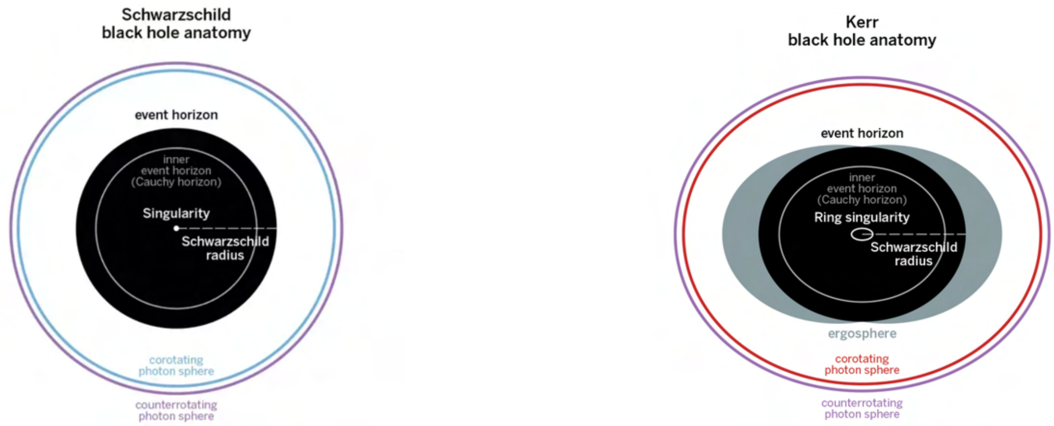

(a) Schwarzschild Black Hole.

(b) Kerr Black Hole.

Figure 6.2: Various regions of a non-rotating and rotating hole.

The horizon of a Kerr black hole occurs at a radius of

$$r_+ = \frac{GM}{c^2} + \left[\left(\frac{GM}{c^2} \right)^2 - \left(\frac{J}{Mc} \right)^2 \right]^{1/2} \tag{6.4}$$

where J is the angular momentum of the hole. The horizon in this case has exactly the same properties as the horizon in the non-rotating case. As we can see from the equation, no black hole is formed if the system has too much angular momentum. We can see that the maximum angular momentum $J = GM^2/c$, and the horizon radius of this maximally rotating black hole is half of that in the Schwarzschild case.

In the case of Kerr black holes, the radii of stable orbits depend on the nature of rotation of orbiting particles with respect to the hole. In the case of a maximally rotating black hole, the last stable orbit for co-rotating objects (rotation is in direction of hole's rotation) is $r = r_+$, while for counter-rotating objects (rotation is opposite to hole's rotation) it is $r = 9r_+$. In between these two radii lies the **static limit**, within which no object can remain at rest relative to background stars. The static limit lies at

$$r_{stat} = \frac{GM}{c^2} + \left[\left(\frac{GM}{c^2} \right)^2 - \left(\frac{J}{Mc} \right)^2 \cos^2\theta \right]^{1/2} \tag{6.5}$$

where θ is the polar angle with respect to the axis of rotation. The static limit is due to the fact that the hole's rotation drags the space and objects around it in the direction of it's rotation. The region between r_+ and r_{stat} is termed as the **ergosphere** and has a number of important properties. While all objects in this region rotate in the same direction as the black hole, they can escape their orbits via the *Penrose process*.

The Penrose process involves the orbiting object splitting into two smaller objects. The momenta of the two objects can be arranged such that one object has net negative energy and spirals into the black hole, allowing the other object to possess greater energy than the original mass had, ejecting it from the orbit. This energy gain of the ejected object comes from the spin of the black hole, and works to slow the spin of the hole. Thus, Penrose showed that the rotational energy of a black hole can be tapped into, and the ergosphere is the region from where the energy is extracted. The fraction of the rest-mass energy of a rotating black hole which can be obtained is

$$1-\frac{1}{\sqrt{2}}\left[1+\left[1-\left(\frac{J}{J_{max}}\right)^2\right]^{1/2}\right]^{1/4}$$

For a maximally rotating black hole, this corresponds to 29% of the rest-mass energy. Larger efficiencies are possible if we consider charged rotating black holes (Kerr-Newman holes). The binding energy of the last stable orbits is given by

$$\left[1-\frac{1}{\sqrt{3}}\right]=0.423 \text{ for co-rotating orbit, } \left[1-\sqrt{\frac{25}{27}}\right]=0.0377 \text{ for counter-rotating orbit}$$

or 42.3% of rest-mass energy of the co-rotating orbit and 3.77% of rest-mass energy of the counter-rotating orbit. The former figure is of great interest because it implies an object spiralling from the last stable co-rotating orbit will release 42.3% of it's rest-mass energy. This is the process by which energy is liberated by friction in accretion discs about black holes and is the probable source of energy in some of the most extreme astrophysical objects. It is also a far more efficient process than nuclear fusion processes, which can release only about 1% of the rest-mass energy.

The singularity in this case is ring shaped, but still possesses zero volume, infinite density and gravitational curvature. The ring singularity lies in the plane of rotation of the hole.

6.2 Properties

Any black hole solution can be completely characterised by just **three** externally observable classical parameters:

- Mass
- Electric charge
- Angular momentum

From just these three parameters all the information about the progenitor of the black hole can be identified. This is commonly called the **No-Hair Theorem**, meaning the black hole has no "hair" sticking out of it that can convey any information about the matter *inside* the black hole, that is permanently inaccessible to external observers, shrouded by the event horizon. However, there exists no rigorous proof for this theorem and therefore it is taken as a conjecture.

An important consequence of the no-hair theorem is the fact that the formed black hole is spherical and contains no information about the shape of the progenitor star. This means that during the implosion of deformed stars, the star somehow manages to rid itself of the deformity and form a spherical hole. The mechanism behind making the hole of the deformed star "hairless" was described by Price's theorem which, put simply, stated that "Whatever can be radiated is radiated" - as the star implodes to beyond the point of the critical radius, the deformity radiates itself away in the form of gravitational waves. The theorem also explains how the black hole loses the magnetic field its progenitor once possessed- it is radiated away in the form of electromagnetic energy. Following from this, the existence of magnetic *monopoles* or charges would mean that the magnetic charge would also be one of the observable parameters stated in the no-hair theorem.

6.3 Active Galactic Nuclei

In 1932, Karl Jansky, who was a radio engineer at Bell Telephone Laboratories, was assigned the task of identifying the source of a background noise prevalent in telephone calls to Europe. After constructing a special radio antenna, Jansky concluded that most of the noise came from thunderstorms, but even in the absence of these storms, a faint static remained. By 1935, he had concluded that most of the static was coming from the central regions of the Milky Way, and were especially strong when the Milky Way was overhead, but still remained after it had sunk below the horizon. Most surprisingly, these radio waves from the central regions of the Milky Way outshone the Sun's radio wave output, despite being over a billion times farther away than the Sun.

Radio maps of the sky were drawn up over the next few years, and they indicated that apart from the central regions of the Milky Way, there were two other bright radio sources- Cyg A and Cas A. Experimental physicists began development of sophisticated radio interferometers, to pinpoint the location of these radio sources, until it was revealed the Cyg A was a **radio galaxy**, with radio emissions coming from two lobes that are over 200,000 light years apart.

In 1960, a radio source named 3C48 was discovered. The region occupied by the source in the sky was extremely small, and optical observations showed the object to look as if it were a star. However, the optical spectrum of the object was unlike any of the stars observed from the Earth or any hot gas encountered by physicists. Over the next two and a half years, more objects showing similar peculiarities were discovered, with astronomers struggling to understand their nature and putting forward contorted interpretations.

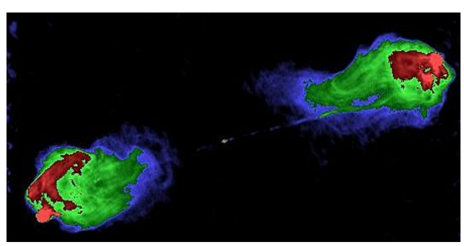

Figure 6.3: Radio image of Cyg A showing its radio-emitting lobes.

The mental block was broken by Maarten Schmidt in 1963, when he noticed that the brightest lines in the spectrum of a similar source 3C273 were the four lines of the Balmer series of the hydrogen spectra, just redshifted off their usual wavelengths by 16%. Similarly, the spectrum of 3C48 revealed spectral lines of magnesium, oxygen and neon redshifted by 37%, meaning that the gas emitting these spectral lines was moving away from the Earth at 37% of the speed of light.

The only explanation behind the high speed of these *quasi-stellar radio sources* or **quasars** could be attributed to the expansion of the universe, and the distance of 3C48 from the Earth to have this high speed would be 4.5 billion light years, following from Hubble's Law. This implied that these quasars shine 100 times more brightly than the brightest galaxies of the Universe, while producing its light in a region of volume 10^{18} times smaller than the light-producing volume of galaxies. Furthermore, the energy efficiency in order to produce this large amount of radio waves through synchroton radiation was unsatisfactorily explained by nuclear conversion or matter-antimatter annihilation.

The idea that black holes in galactic cores may power these radio galaxies and quasars was first put forward by Edwin Salpeter and Yakov Zeldovich. However the black holes powering these objects are not ordinary- they are gigantic black holes with masses many million times that of the Sun. The massive amount of energy generated is through the frictional heating of the accretion disc of the black hole. The small size of the accretion disc in comparison to the size of the galaxy explained the small region from where electromagnetic radiation was emanating in the case of quasars, and the steady nature of the lobes in radio galaxies was explained by the nature of black holes to behave like a gyroscope and maintain a steady spin axis.

However, a key requisite for the generation of radio waves through synchroton radiation is the existence of a magnetic field which, by the no-hair theorem, cannot be possessed by a black hole. But the super-massive black holes at the heart of galaxies do indeed possess magnetic field. The key here is the fact that the magnetic field is not generated by the black hole, but the spinning accretion disc around it. The magnetic field, anchored in the disc, rotates along with the black hole and flings plasma from the disc along the field lines, forming twin magnetised jets. An interesting variation of this process is known as the *Blandford-Znajek process.*

In the Blandford-Znajek process, the jets shoot out along the hole's spin axis, their direction anchored by the gyroscopic spin of the hole, and the power of these jets comes from the hole's enormous rotational energy. But in this case the hole's horizon is threaded by magnetic fields, which appears to be in violation of the no-hair theorem, but this is not the case. The magnetic field, like the previous case, is generated by the accretion disc, and is confined to region of the black hole by the disc itself. The field lines cannot be radiated away as they are confined by the hot gas to the region within the last stable circular orbit (for co-rotating objects).

Even though both quasars and radio galaxies are powered in the same way by a super-massive black hole, there exists a key difference between the two. The light of a quasar appears to come from an extremely luminous star-like object, with a size 1 light month or less, while in the case of radio galaxies, the light comes from a region of a large assemblage of stars, over 100,000 light years in size. The variation between the two is due to the fact that the central black hole of a quasar is fueled by the accreting gas at an extremely high rate, and the high frictional heating provides an

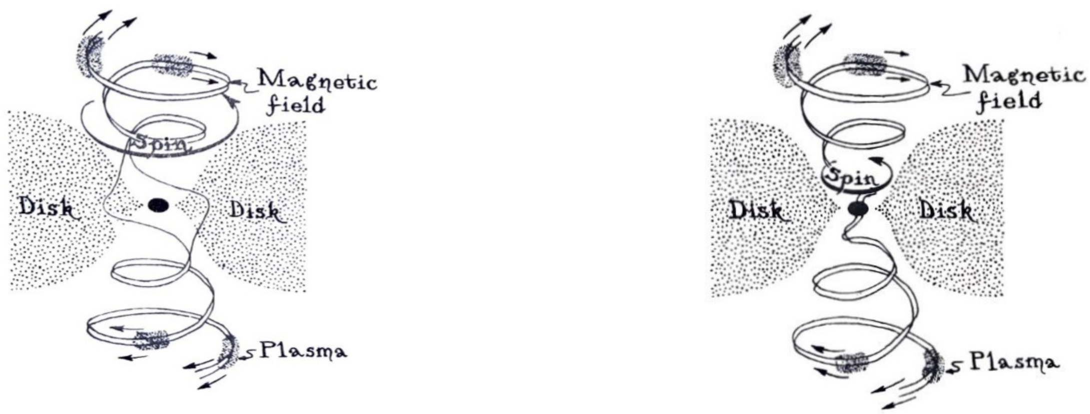

(a) Magnetic field anchored in disc.

(b) Blandford-Znajek process.

Figure 6.4: Two methods behind powering the twin jets.

optical output greater than all the stars in the galaxy put together, making it look quasi-stellar, or star-like. In radio galaxies, the black hole is fed at a quiescent rate. Therefore, what is observed is not the accretion disc, but the enormous radio-emitting lobes that are shot through the galaxy and into intergalactic space.

6.4 Black Hole Thermodynamics

In November 1970, Stephen Hawking had figured out an interesting feature of black holes. Using a concept of absolute and apparent horizons, he showed that in a system of black holes, if you measure the sum of areas of all absolute horizons, then at a later instant, this sum of areas cannot have decreased- it can only stay the same, or increased, provided no black hole has "moved" out of the system. Basically, the areas of absolute horizons is always non-decreasing.

While Hawking noticed a remarkable similarity between his law of areas and the second law of thermodynamics, which states that the total entropy of the system is non-decreasing, he took it to be a mere coincidence. To him it was non-intuitive to claim that the surface area of a black hole is its entropy, due to the seemingly lack of randomness associated with black holes, which are determined by just three parameters. However, Jacob Bekenstein argued that the black hole area is, in some sense, its entropy. He was convinced that if black holes possessed no entropy it would lead to a violation of the second law of thermodynamics, as any entropy associated with an object would be lost as it fell through a black hole.

Noting these similarities between black hole physics and thermodynamics proved fruitful, as in 1972 Bekenstein, along with other physicists, managed to draw out a set of four **laws of black hole thermodynamics**, which are analogous to the laws of thermodynamics.

- *Zeroth Law:* The horizon of a stationary black hole has constant surface gravity. This is analogous the corresponding law of thermodynamics which states that a system in thermal equilibrium possesses constant temperature.
- *First Law:* This law relates the change of energy of a stationary black hole with the change of area, angular momentum and electric charge, akin to the first law of thermodynamics.
- *Second Law:* The horizon area is a non-decreasing function of time.

$$\frac{dA}{dt} \geq 0$$

- *Third Law:* It is not possible to form a black hole with zero surface gravity.

From these laws, it was possible to confirm Bekenstein's conjecture regarding the relation between black hole area and entropy, and it was obtained as:

$$S_{BH} = \frac{k_B}{4{l_P}^2} A \tag{6.6}$$

where k_B is Boltzmann constant, and l_P is the Planck length, given by

$$l_P = \sqrt{\frac{G\hbar}{c^3}}$$

Similarly, it was possible to define a surface temperature for a black hole, given by

$$T = \frac{\hbar c^3}{8\pi G M k_B} \approx \frac{10^{-7}}{(M/M_\odot)}\ \mathrm{K} \tag{6.7}$$

The outcomes of these laws, however, led to many, including Hawking, disregarding the Bekenstein conjecture, as the definition of a surface temperature for a black hole must imply that black holes must radiate, following from thermodynamics. But that should not be possible, as nothing can escape to the outer Universe from within the event horizon. While many physicists came up with explanations regarding mechanisms allowing black holes to radiate, it was Hawking himself who later gave a concrete explanation behind the mechanism.

In 1973, Hawking met Zeldovich who had proposed a way by which rotating black holes could radiate. At the heart of his idea were vacuum fluctuations- random generation of virtual matter-antimatter pairs by borrowing energy from the Universe, and the emission of the borrowed energy by annihilation of these pairs. From these insights, Hawking devised the mechanism behind **Hawking radiation**.

In his mechanism, vacuum fluctuations generate a virtual pair just beyond the horizon itself. One of the generated particles fall into the hole, while the other manages to escape. The infalling particle bears negative energy (in order to conserve total energy), causing the black hole to lose mass, while to an external observer, it would appear that the black hole has emitted or radiated a particle. This radiation supersedes the second law of black hole thermodynamics.

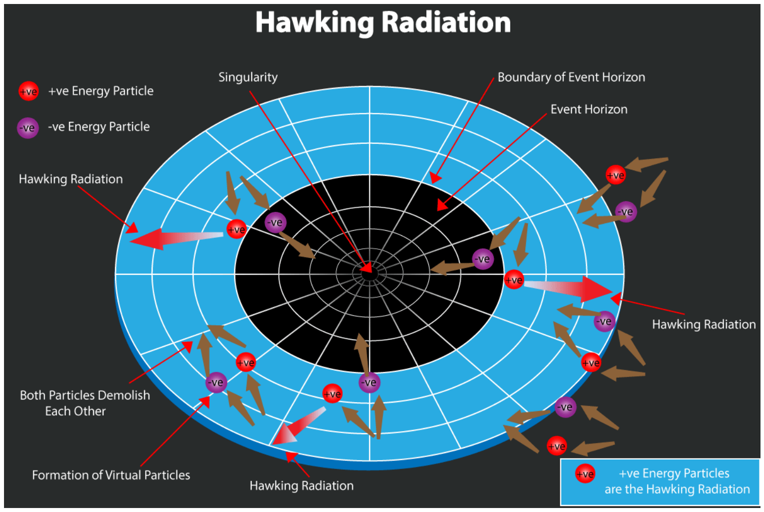

Figure 6.5: Physical insight into Hawking Radiation.

An outcome of Hawking radiation is the fact that black holes "evaporate" and have a limited time-span. However, the process is so slow that it take an extraordinarily large amount of time for a black hole to fully evaporate. A solar mass black hole would take 10^{64} years to fully evaporate, while supermassive black holes can take more than 10^{100} years. At this end, the Universe would be a cold, dark place, with all stars having imploded to or consumed by black holes, and white dwarfs having become cold black dwarfs.

References

- *High Energy Astrophysics* by Malcolm S. Longair.
- *An Introduction to Astrophysics* by Baidyanath Basu.
- *Black Holes and Time Warps* by Kip S. Thorne.
- *Senior Astrophysics* course slides at University of Sydney by Helen Johnston available here.
- *Stellar Evolution* course slides at University of Oxford by Tony Lynas-Gray available here.
- *Stellar Structure and Evolution* notes by Warrick Ball at the Indo-German Winter School on Solar and Stellar Astrophysics available here.

Image References

- *Google Images*: 1.1, 2.1, 2.2, 2.3, 3.1, 3.3, 3.5, 5.1, 5.2, 6.2a, 6.2b, 6.3, 6.5.
- *High Energy Astrophysics*, Longair: 2.7, 3.4, 4.2, 4.3, 5.3.
- *An Introduction to Astrophysics*, Basu: 2.4.
- *Black Holes and Time Warps*, Thorne: 4.4, 6.1, 6.4a, 6.4b.
- *Senior Astrophysics*, University of Sydney: 2.5, 2.6, 2.8, 2.9, 3.2, 4.1.